A. K. TUKAY

ATILIM UNIVERSITY 2023

ADVANCED PERIODONTAL TOOTH EXTRACTION WOUND HEALING MATERIALS: ELECTROSPUN CORE-SHELL PCL/PCL NANOFIBERS

THE GRADUATE SCHOOL OF NATURAL AND APPLIED SCIENCES
OF
ATILIM UNIVERSITY

ARI KUTLUG TUKAY

A MASTER OF SCIENCE
THESIS
IN
THE DEPARTMENT OF METALLURGICAL AND MATERIALS ENGINEERING

MAY 2023

ADVANCED PERIODONTAL TOOTH EXTRACTION WOUND HEALING MATERIALS: ELECTROSPUN CORE-SHELL PCL/PCL NANOFIBERS

A THESIS SUBMITTED TO
THE GRADUATE SCHOOL OF NATURAL AND APPLIED SCIENCES
OF
ATILIM UNIVERSITY

BY

ARI KUTLUĞ TUKAY

IN PARTIAL FULFILLMENT OF THE REQUIREMENTS
FOR
THE DEGREE OF MASTER OF SCIENCE
IN
THE DEPARTMENT OF METALLURGICAL AND MATERIALS ENGINEERING

MAY 2023

Approval of the Graduate School of Natural and Applied Sciences, Atılım University.

_____

Prof. Dr. Ender KESKINKILIC
Director

I certify that this thesis satisfies all the requirements as a thesis for the degree of **Master of Sciences in Department of Metallurgical and Materials Engineering, Atılım University.**

_____

Prof. Dr. Ender KESKINKILIC
Head of Department

This is to certify that we have read the thesis "ADVANCED PERIODONTAL TOOTH EXTRACTION WOUND HEALING MATERIALS: ELECTROSPUN CORE-SHELL PCL/PCL NANOFIBERS" submitted by "ARI KUTLUG TUKAY" and that in our opinion it is fully adequate, in scope and quality, as a thesis for the degree of Master of Science.

_____

Prof. Dr. Hilal TURKOGLU SASMAZEL
Supervisor

Examining Committee Members:

Prof. Dr. Bilgehan OGEL
Metallurgical and Materials Eng., METU _____

Prof. Dr. Hilal TURKOGLU SASMAZEL
Metallurgical and Materials Eng., Atılım University _____

Asst. Prof. Dr. Doruk DOGU
Metallurgical and Materials Eng., Atılım University _____

Date: *30.05.2023*

I hereby declare and guarantee that all data, knowledge and information in this document has been obtained, processed and presented in accordance with academic rules and ethical conduct. Based on these rules and conduct, I have fully cited and referenced all materials and results that are not original to this work.

Name, Last Name : Ari Kutlug, Tukay

Signature :

ABSTRACT

ADVANCED PERIODONTAL TOOTH EXTRACTION WOUND HEALING MATERIALS: ELECTROSPUN CORE-SHELL PCL/PCL NANOFIBERS

TUKAY, Ari Kutlug
M.S., Metallurgical and Materials Engineering Department
Supervisor: Prof. Dr. Hilal Turkoglu Sasmazel

May 2023, 90 pages

The aim of this study is to ensure the production of core-shell PCL/PCL nanofibers using electrospinning technique and to contribute to the acceleration of the healing of periodontal wound areas by coating the surfaces of the produced nanofibers with DAP monomer using dielectric barrier discharge plasma method.

Nanofibrous scaffolds were produced using the core-shell electrospinning method. The produced nanofibers were subjected to the DBD plasma process for 1 min., 3 min., and 5 min., and their surfaces were coated with DAP monomer during surface modification. Characterizations of the samples were performed using contact angle (CA) measurements, scanning electron microscopy (SEM), transmission electron microscopy (TEM), Fourier transform infrared spectroscopy (FTIR), and tests for gas permeability, mechanical properties, thickness measurements, PBS absorption and shrinkage analysis were conducted for the produced core-shell PCL/PCL nanofibers. Group 1, resulting from the use of the more viscous chloroform solvent in the shell, and group 2, produced by using the higher viscosity chloroform solvent in the core, were compared. The average fiber diameter values were calculated as 1.252 ± 0.422 for PCL/PCL group 1 produced by the electrospinning method, and after surface modifications, 1.366 ± 0.211 for 1 min., 1.369 ± 0.129 for 3 min., and 1.372 ± 0.230

for 5 min. For group 2, the average fiber diameter values were; 2.039 ± 0.503, 2.152 ± 0.705 for 1 min., 2.156 ± 0.711 for 3 min., and 2.160 ± 0.602 for 5 min. surface-treated samples. The FTIR analyses of core-shell PCL/PCL nanofibers also showed the characteristic polymer peaks formed before and after the DBD plasma surface coating with added DAP monomer.

Cell culture studies were performed with the L929 mouse fibroblast cell line. The biocompatibility performance of the nanofibers was determined by the MTT test, fluorescence staining test, and SEM analysis. The results indicated that group 2, produced by the electrospinning method and whose surfaces were coated with DAP monomer using the DBD plasma method for 5 minutes, increased cell viability and proliferation on/within the nanofibrous structures in this study.

Keywords: Poly (ε-Caprolactone) (PCL), Core-Shell Electrospinning, Periodontal Wound Healing Materials, DBD (Dielelectric Barrier Discharge Plasma), DAP (Diethyl Allyl Phosphate).

ÖZ

İLERİ PERİODONTAL DİŞ ÇEKİMİ YARA YERİ İYİLEŞME MALZEMELERİ: ELEKTROEĞİRİLMİŞ ÇEKİRDEK-KABUK PCL/PCL NANOFİBERLER

Tukay, Arı Kutluğ
Yüksek Lisans, Metalurji ve Malzeme Mühendisliği Bölümü
Tez Yöneticisi: Prof. Dr. Hilal Türkoğlu Şaşmazel

Mayıs 2023, 90 sayfa

Bu çalışmanın amacı; elektroeğirme tekniği kullanarak çekirdek-kabuk PCL/PCL nanofiberlerin üretilmesinin sağlanması ve üretilen nanofiberlerin yüzeyleri dielektrik barrier discharge plazma yöntemi ile DAP monomeri kaplanarak, periodontal yara yeri bölgelerinin iyileşmesinin hızlandırılmasına katkı sağlanmasıdır. Nanofiber yapılı iskeletler çekirdek-kabuk elektroeğirme yöntemi ile üretilmiştir. Üretilen nanofiberler 1 dk., 3 dk. ve 5 dk. olarak DBD plazma işlemine tabi tutulmuş ve yüzey modifikasyonu sırasında yüzeyleri DAP monomeri ile kaplanmıştır. Örneklerin karakterizasyonları, temas açısı (CA) ölçümleri, taramalı elektron mikroskobu (SEM), geçirimli elektron mikroskobu (TEM), Fourier dönüşümü kızılötesi spektroskopisi (FTIR) ve ayrıca üretilen çekirdek-kabuk PCL/PCL nanofiberler için gaz geçirgenlik testi, mekanik testi, kalınlık ölçümleri, PBS emilim ve büzülme testleri gerçekleştirilmiştir. Viskozitelik bakımından daha fazla vizkoziteye sahip kloroform çözücünün kabukta kullanılması ile oluşturulan Grup-1 numuneleri ve kloroform çözücünün çekirde kullanılması ile üretilen Grup-2 numuneleri karşılaştırılmıştır. Ortalama fiber çap değerleri, elektroeğirme yöntemi ile üretilmiş PCL/PCL grup 1 için 1.252 ± 0.422 ve yüzey modifikasyonları sonrasında 1 dakikalık için 1.366 ± 0.211, 3

dakikalık için 1.369 ± 0.129 ve 5 dakikalık için 1.372 ± 0.230 olarak hesaplanmıştır. Grup 2 için ortalama fiber çap değerleri; 2.039 ± 0.503, 1 dakikalık için 2.152 ± 0.705, 3 dakikalık için 2.156 ± 0.711 ve 5 dakikalık yüzey işlemine tutulmuş numuneler için 2.160 ± 0.602 olarak hesaplanmıştır. Çekirdek-kabuk PCL/PCL nanofiberlerin FTIR analizleri, DAP monomeri eklenerek DBD plazma yüzey kaplaması öncesinde ve sonrasında oluşan karakteristik polimer zirvelerini de göstermiştir. Hücre kültürü çalışmalarında L929 fare fibroblast hücre hattı ile çalışılmıştır. Nanofiberlerin biyouyumluluk performansları MTT testi, flüoresans boyama testi ve SEM analizi ile belirlenmiştir. Sonuç olarak; bu çalışmada oluşturulan Grup-2'nin elektroeğirme yöntemi ile üretilmiş ve yüzeyleri 5 dakika boyunca DBD plazma yöntemi kullanılarak DAP monomeri ile kaplanmış PCL/PCL nanofiberlerin nanofiber yapılar üzerinde/arasında hücre canlılığını ve proliferasyonunu arttırdığı gösterilmiştir.

Anahtar Kelimeler: Poli (ε-Kaprolakton) (PCL), Çekirdek-kabuk elektroeğirme, Periodontal Yara Yeri İyileştirme Malzemesi, DBD (Dielektrik Bariyer Deşarj Plazma), DAP (Dietil Alil Fosfat).

This work is dedicated to my beloved mother, dentist Tünay TUKAY ...

ACKNOWLEDGMENTS

First and foremost, I would like to express my deep gratitude to my advisor Prof. Dr. Hilal TURKOGLU SASMAZEL, who has always been by my side and has been an incredible mentor. I am greatly thankful to you for encouraging my research and for contributing to my growth as a research scientist. Your advice on my career and your guidance in life have been invaluable to me. I could not have imagined having a better advisor and mentor for my master's study.

I would like to extend my deepest thanks to the rest of my thesis committee, Prof. Dr. Bilgehan OGEL and Asst. Prof. Dr. Doruk DOGU, for their endless support and contributions.

I am deeply grateful to my dearest friend Barkan Kagan DURUKAN, who has always been by my side and never withheld his support from me.

I am deeply grateful to my beloved wife Atty. Betul OZTULUM TUKAY, who has always held my hand, supported my academic studies, and made me feel loved with her life advice. Her place in my life is very important to me.

I wish to express my deepest love and gratitude to my mother-in-law Serap HIRKA and my brother-in-law Yasar OZTULUM, who have always been by my side in every moment and every condition, enriching my life and loving me unconditionally.

Lastly, I wish to convey my endless love and gratitude to my unique father D.D.S. Ph.D. Ender TUKAY, who instilled in me the values that make me who I am, who has never let go of my hand, who has believed in me forever, who has always stood by me, and whose contributions and efforts to this study are infinite. And to my beloved mother, Dentist Tünay TUKAY, who never ever let go of my hand until the last moment of her life, who remains eternally in my heart and mind, and who I know is watching over me from heaven. I lost her on April 26, 2023, and I would like to express my eternal love and gratitude to her.

TABLE OF CONTENTS

LIST OF TABLES

LIST OF FIGURES

LIST OF ABBREVIATIONS

PCL	Poly (Ɛ-Caprolactone)
E.S.	Electrospinning
C-S	Core-Shell
CA	Contact Angle
ATR – FTIR	Attenuated Total Reflection Fourier Transform Infrared
SEM	Scanning Electron Microscope
TEM	Transmission Electron Microscope
FDA	U.S. Food and Drug Administration
DAP	Diethyl Allyl Phosphate
DBD	Dielectric Barrier Discharge Plasma
Ar	Argon
TCPS	Tissue Culture Polystyrene
PBS	Phosphate Buffer Saline
WVTR	Water Vapor Transmission Rate
DCM	Dichloromethane

CHAPTER 1

Introduction

The objective of periodontal therapy and tooth extraction surgery in dentistry is to reduce or eliminate inflammation caused by bacteria and plaque, repair damage caused by periodontal disease, and revitalize periodontal tissues. If a tooth is damaged owing to a fracture or severe decay and cannot be saved with a filling or crown, the dentist may determine that extraction is the best course of action. Teeth that are not supported by sufficient bone tissue because of periodontal disease are often extracted. Additionally, if a tooth does not respond to root canal treatment and becomes infected, extraction may also be necessary. After periodontal treatment, such as tooth extraction surgery or bone surgery, the healing process typically involves the growth of long junctional epithelium or connective tissue that adheres to and repairs [1]. Healing through regeneration results in complete restoration of the lost periodontium [2]. Effective regeneration requires an appropriate combination of signaling molecules, precursor stem cells, and extracellular matrix-mimicking structures [3].

Poly (ε-caprolactone) (PCL) is a semi-crystalline polymer that is biodegradable, hydrophobic, and it has been approved by the FDA. It has good mechanical properties, is inexpensive, and easy to produce. Compared to other polymers, PCL has excellent elasticity but a lower tensile strength. This makes it an ideal material for biomedical applications. PCL has been shown to provide stability in electrospun materials and to have the necessary topographical features for endothelial cell attachment and migration. In addition, PCL has been reported to reduce fibrosis during wound healing. PCL scaffolds with porous and fibrous structures have lower tensile strength and elastic modulus than PCL, which has a tensile strength of approximately 25-43 MPa and an elastic modulus of approximately 330-360 MPa [5].

PCL polymers not only promote the attachment and growth of human mesenchymal stem cells (MSCs), but also support the differentiation of osteogenic and periodontal tissues [4]. Additionally, PCL-based electrospun materials have been used in many dental research and applications because of their high permeability [5]. PCL has a slow

degradation rate and is hydrophobic, making it a good fit for use in regenerative processes in tissue engineering. However, their weak cellular activity and sensitivity to plasma proteins make them insufficient for their own use. As a result, PCL is often used in combination with other polymers during electrospinning to increase the degradation rate, improve hydrophilicity, and enhance biocompatibility [6].

Biocompatibility is an essential characteristic of all tissue scaffolds. Developing tissue scaffolds that imitate the extracellular matrix (ECM) through an appropriate production method and the use of a suitable material are crucial for the utilization of PCL in tissue engineering. In terms of biocompatibility, the PCL polymer, with its low immunogenicity and optimal degradation, is a commonly chosen polymer for tissue scaffold preparation. Furthermore, the ability of PCL polymers to work well with other synthetic and natural polymers is important to ensure that the desired characteristics are obtained during the preparation of tissue scaffolds.

Electrospinning is used for the production of PCL tissue scaffolds for use in tissue engineering. It involves rapid prototyping and the creation of porous nanofiber structures. The basic design of the electrospinning process was divided into four main parts. They are solution preparation, electrospinning setup, process parameters, and types of electrospinning. The components of an electrospinning device include a syringe filled with a polymer solution metallic needle, power source and metallic collector or mandrel with variable shapes.

The electrospinning technique applies electric charges to the polymer solution using a metallic needle. This movement of the polymer solution created instability, and the charges on the droplets causes the polymer solution to flow in the direction of the electric field. The increase in the electric field helps the droplets to deform into a cone shape, and ultrafine nanofibers are produced and collected on a metallic collector.

In general, the flow of current through a solution via a metallic needle from a high-voltage power source results in the deformation of a spherical droplet (in the form of a Taylor cone) and the formation of ultra-fine nanofibers at a critical voltage [7].

A stable charge jet can only be created by electrospinning using a polymer solution with sufficient cohesive forces. During this process, the internal and external forces

work together to direct the liquid jet towards the collector. This directional motion allows for the stretching of polymer chains within the solution and sliding past each other, resulting in the formation of small-diameter fibers referred to as nanofibers [8].

The electrospinning process is mainly affected by three factors. These factors included the applied electric field, distance between the needle and collector, flow rate, and diameter of the metallic needle. The critical value of the applied voltage varies from one polymer to another. These factors include the electrical parameters required to perform the electrospinning process, solution ratios, and environmental parameters.

An increase in the applied voltage leads to the formation of smaller-diameter nanofibers, which are connected to the electrical surface tension of the polymer solution owing to charge thrusting in the polymer jet. An increase beyond the critical value at the applied voltage causes bead-like nanofibers to form. The increase in the diameter and formation of bead-like nanofibers are proportional to the decrease in the size of the Taylor cone for the same flow rate and an increase in the jet speed. The distance between the metallic needle tip and the collector plays an important role in determining the morphology of the electrospun nanofibers. Similar to the applied electric field, viscosity, and flow rate, the distance between the metallic needle tip and collector also varies depending on the polymer system. The morphology of the nanofibers is easily affected by distance because it depends on the accumulation time. The solution parameters included the solvent, polymer concentration, viscosity, and solution conductivity. Many research groups have examined the effect of the distance between the needle tip and collector and found that when the distance was short, wide and flawed nanofibers were formed; however, as the distance increased, the diameter of the nanofibers decreased. However, there are also studies in which no effect on the morphology of the nanofibers was observed as a result of changes in the distance between the metallic needle and collector [9].

The environmental parameters included the relative humidity, pressure, and temperature. In addition, the rate of evaporation or instability can also affect the morphology of nanofibers [10]. Therefore, it is necessary to maintain a critical distance to prepare the electrospun nanofibers. Any changes on either side of this critical distance affect the morphology of the nanofibers [11].

All these parameters directly affect the production of porous electrospun polymer fibers. Therefore, it is necessary to optimize all these parameters to produce the desired polymer nanofibers. Nanofiber membranes equipped with biological signals through electrospinning have the potential to be used in directed tissue regeneration by providing an optimal microenvironment for cell differentiation and proliferation [12]. In the electrospinning technique, electrostatic forces are used to convert a charged polymer solution into a nanometer-sized fiber network. While traditional electrospinning techniques use only one polymer, multiple component nanofibers can be produced using more complex methods, such as coaxial electrospinning [13]. Coaxial electrospinning is a technique that allows the production of "core-shell" fibers made of a "core" consisting of a drug or growth factor and/or protein and a "shell" polymer that provides mechanical properties. This enables the direct inclusion of biologically active molecules into the core component, allowing for the controlled release of the desired drug or protein [14]. In recent coaxial electrospinning studies, a multifunctional electrospinning core-shell nanofiber membrane capable of electrospun periodontal ligament stem cells (PDLSCs), fibroblasts cells and osteoblasts cells have been developed. These core-shell nanofibers have been used for periodontal regeneration by providing a mechanical barrier for epithelial growth. Furthermore, because core-shell nanofibers can also serve as a delivery vehicle for biologically active molecules, they have also been used in different periodontal studies in dentistry, as they can induce cell differentiation and bone formation in the periodontal area [15].

The literature has shown that the use of PCL polymer in the shell region of nanofiber structures produced using the coaxial electrospinning method creates the basic structure of periodontal wound healing materials. *S. aureus* and *C. albicans*, which are the most commonly found bacteria species in the oral microbiome, are the bacteria responsible for causing infections around implants. These bacteria play a role in peri-implantitis infections, which are frequently encountered in dental implants, limit the long-term use of implants, and cause complications in treatment [16]. In addition, platelet formation and protein adsorption due to surface chemistry and topographical structures are observed in dental implants and dental wound materials [17]. Studies have shown that complications can be prevented by using surfaces with amphoteric properties. The acidic and basic groups that create amphoteric properties increase the

water-holding capacity of the surface, thus creating a barrier for water molecules to prevent protein adsorption and ensure healthy cell adhesion [18]. When monomers containing phosphate and phosphite groups are polymerized on the surface using the plasma modification method, hydrophilic and amphoteric surfaces are obtained. Platelet formation has also been observed to decrease on these surfaces.

Diethyl allyl phosphate (DAP), a monomer containing phosphate groups, has been found to create acidic (-OH) and basic (-PH) functional groups through the activation of allyl groups during plasma modification [18-19]. This results in a surface that exhibits both acidic and basic properties [18]. Literature has shown that the use of DAP monomers can prevent protein adsorption and promote healthy cell attachment to surfaces with both acidic and basic properties [18]. In a previous study, it was found that DAP monomers create different functional groups with different parameters for DBD plasma modification. The principle of DBD plasma modification shows that the frequency of charging and discharging cycles causes different bonds in the DAP monomer to break, creating different radical groups [19]. The study found that low charging-discharging cycles produced the desired phosphate groups [19].

Based on these studies, the surfaces of the PCL/PCL core-shell nanofibers to be produced will be coated with DAP monomers using the DBD plasma method, making it amphoteric. This prevents the adsorption of harmful bacteria while allowing healthy cell attachment to the surface.

The core-shell type PCL/PCL nanofibers produced using the coaxial electrospinning method have not been subjected to any plasma polymerization method using DAP monomer to modify the surface, making the project (thesis) unique in this regard.

Plasma surface modification allows the development of materials that are suitable for desired applications by improving only the surface properties without changing the structural integrity of the materials. The advantages of plasma surface modification are as follows: it is cheap and repeatable, it coats surfaces with different geometries, it provides a homogeneous coating, and it improves and functionalizes the tribological properties of the surface.

There are various plasma surface modification methods such as low-pressure radio frequency plasma, spark discharge plasma, microwave plasma, arc plasma, and dielectric barrier discharge (DBD) methods used for the soft tissue applications [20]. Among these plasma modifications, DBD plasma modification is more advantageous and efficient than vacuum- and thermal-based plasma modification methods. Therefore, the DBD plasma method is preferred for plasma coatings, thin-film storage, and material surface modifications [21]. In the DBD plasma method, plasma is produced at the desired frequency cycles by placing a dielectric barrier between the two electrodes, and in this way, the desired material surfaces are coated. The dielectric barrier has two functions within the system: to control the amount of charge generated between the two electrodes by forming a single microdischarge and to ensure that the generated microdischarges are homogeneously distributed over the entire electrode surface area. Using the DBD plasma method, an average energy of 0-20 eV is produce.

The bonds formed by polymers or monomers have a low energy of 10 eV, and the DBD breaks these bonds and enables the formation of high-energy particles [22]. The free electrons produced by the charge created between the two electrodes in the DBD plasma accelerate and collide with the charged gas molecules in the system, causing fragmentation and ionization of the gas molecules. These thermodynamically unstable ionized gas molecules then attach to the surface of the material in the system and become stable, thereby completing the DBD plasma modification process [23].

The DBD plasma modification method has three main parameters: applied voltage, application time, and gas flow rate. The applied voltage parameter brake the bonds of the gas molecules to be coated. The application time parameter determines the probability of collision between the ionized gas particles and the material surface. The number of active groups produced in the DBD plasma is controlled by the gas flow rate parameter. By optimizing these parameters, functionalization of material surfaces can be achieved without dependence on the surface geometry of the material [19]. Based on this information, the core-shell-type PCL/PCL nanofibers produced by coaxial electrospinning were coated with DAP using the DBD plasma method.

The main objective of this study is to facilitate the recovery of periodontal wounds by developing a coaxial electrospun nanofiber structure with a core-shell design that

mimics the extracellular matrix (ECM) and to accelerate the healing process. The nanofiber surfaces were coated with DAP monomers using the DBD plasma method, and the amphoteric nature of the monomer was expected to enable the attachment of surrounding tissues while preventing the adsorption of bacteria and proteins. No prior studies have reported the production of a wound-healing material for periodontal wound healing using core-shell PCL/PCL and DAP monomers, including physical, chemical, and biological characterization of the structure. This study contributes to the literature by introducing a new biomaterial that can accelerate periodontal wound healing.The research question behind this project was to investigate the feasibility of using a core-shell type PCL/PCL nanofiber structure coated with DAP monomer using the DBD plasma method, which has a PCL polymer in its structure and provides controlled biodegradation, mimics the extracellular matrix, and enables healthy cell attachment and proliferation on its surface as a periodontal wound healing material.

In this study, the goal was to create core-shell PCL/PCL nanofibers using electrospinning and modify their surface with DBD plasma and diethyl allyl phosphate (DAP) monomer for processing times of 1, 3, and 5 min. These nanofibers are intended for use in applications such as thermal and dental wound healing. Three approaches are used in this study. The first approach involves electrospinning a blend of DCM in the core and chloroform in the shell to create the core-shell PCL/PCL nanofibers. The second approach compares the electrospinning parameters while considering the viscosity changes of the core-shell PCL/PCL nanofibers, using chloroform in the core and DCM in the shell. The third approach involves the use of DBD plasma to modify the surface of electrospun core-shell PCL/PCL nanofibers with DAP monomers for 1, 3, and 5 min. The optimal solution and process parameters were determined through literature review and optimization experiments. The nanofiber morphology was analyzed using SEM and TEM, and their wettability was determined using CA measurements. Chemical analysis was performed using FTIR and WVTR on the electrospun core-shell PCL/PCL nanofibers and the nanofiber surface modified by DBD plasma with DAP monomer for 1, 3, and 5 min. Other tests included thickness measurements, mechanical property analysis, PBS absorption, in vitro degradation, and WVTR studies. Finally, the interaction between the candidate nanofibers and cells was studied in vitro for 7 days using the L-929 cell line.

CHAPTER 2

Literature Survey

2.1. Dental Tissue Engineering

Dental tissue engineering is a growing area of research focused on the development of new treatments for oral and facial diseases and disorders. This multidisciplinary field combines principles from biology, material science, and engineering to create functional and biocompatible materials that can be utilized to replace or regenerate damaged or lost oral tissues. The ultimate goal is to enhance patient outcomes and quality of life by providing effective treatment for oral and facial conditions [24].

A key aspect of dental tissue engineering is the use of undifferentiated stem cells with the ability to develop into various cell types found in the oral cavity, such as odontoblasts and cementoblasts. This makes stem cells an appealing option for use in dental tissue engineering, as they have the potential to regenerate lost or damaged tooth structures [25-26]. Stem cells can be obtained from several sources, including dental pulp, periodontal ligament, and adipose tissue, and then differentiate into the desired cell type. Once differentiated, these cells can be combined with a suitable scaffold material and implanted in the affected area to stimulate tissue regeneration [26].

Scaffolds are important components of dental tissue engineering. A scaffold is a three-dimensional structure that provides a physical support system for cell attachment, growth, and differentiation. Scaffolds can be made from a variety of biocompatible materials, such as ceramics, polymers, or natural materials, and are designed to mimic the physical and chemical properties of the tissues they are intended to replace. The scaffold provides a supportive environment for cell growth and differentiation and can be used to deliver growth factors and other biological signals that direct cell behavior and promote tissue regeneration [27].

Jawbone loss, a common problem in the oral cavity caused by periodontal disease or tooth loss, can also be addressed by dental tissue engineering. Scaffolds filled with bone marrow aspirate or other cell-containing sources can be used to regenerate

jawbone tissue. These scaffolds can be designed to imitate the structure and composition of the natural jawbone and can be implanted into the affected area to stimulate the formation of new bone tissue [28].

Along with stem cells and scaffolds, dental tissue engineering involves the use of growth factors, gene therapy, and other biological signals to promote tissue regeneration. Growth factors can be used to stimulate the growth and differentiation of stem cells and direct their behavior towards the formation of new tissues. Gene therapy, however, involves delivering therapeutic genes into cells to promote tissue regeneration and repair [29-30].

In conclusion, dental tissue engineering is a rapidly growing field with great potential for the treatment of oral and facial diseases and disorders. Researchers are using the principles of biology, materials science, and engineering to develop new and innovative approaches for the regeneration of damaged or lost oral tissues. Despite the need for additional research, current advancements in stem cell biology, material science, and engineering offer great potential for the development of effective therapies for the oral cavity.

2.1.1. Dental Tissue Scaffolds

Dental tissue scaffolds are an important aspect of tissue engineering in dentistry and oral surgery. These scaffolds are three-dimensional structures that provide a supportive framework for the growth and regeneration of dental tissues, such as teeth, gums, and jaw bones. They are typically made from biological materials such as extracellular matrix (ECM) proteins or biocompatible synthetic materials [31].

Various fabrication techniques have been developed for the production of dental tissue scaffolds, which can be divided into two main categories as conventional and advanced techniques [32]. Conventional methods, such as electrospinning, solvent casting, particulate leaching, and freeze drying, are capable of producing scaffolds with interconnected porous structures but offer limited control over pore size, shape, and distribution. Advanced techniques such as electrospinning and rapid prototyping allow for greater control over the structure of the scaffold, including the creation of internal channels, and offer the potential for more precise and accurate scaffold design [33].

The development of advanced fabrication techniques has led to the emergence of biofabrication, which involves the production of complex living and nonliving biological products. This field has the potential to revolutionize the manufacturing industry and significantly contribute to the advancement of tissue engineering strategies, including dental tissue engineering.

In conclusion, dental tissue scaffolds play a crucial role in promoting the growth and regeneration of dental tissues, and are an important aspect of tissue engineering in the field of dentistry. The use of advanced fabrication techniques such as electrospinning and rapid prototyping offers new possibilities for the design and production of these scaffolds, leading to improved outcomes for patients undergoing dental treatments and procedures [34].

2.1.2. Natural and Synthetic Polymeric Dental Tissue Scaffolds

Scaffold design and fabrication are crucial areas of research in dentistry, tissue engineering, and regenerative medicine. Scaffolds are essential components in tissue repair and regeneration and have been extensively studied over the past 20 years. Scaffolds are three-dimensional, porous biomaterials that serve various functions, including promoting cell-biomaterial interactions, facilitating the transport of nutrients and gases for cell survival, controlling tissue regeneration by degradation at a controlled rate, and minimizing inflammation and toxicity in the body [30]. Polymeric scaffolds offer better control over properties such as strength, porosity, and degradation rate, and can be produced more consistently during development. Biological scaffolds are obtained from animal or human tissues, whereas synthetic scaffolds are derived from polymers. Some scaffolds exhibit biological activity and are used to regenerate tissues and organs that cannot be regenerated on their own [31]. Initial studies on tissue regeneration using scaffolds involve the use of the dermis as a scaffold in animals and humans, resulting in the regeneration of peripheral nerves and conjunctival tissue across unprecedented gaps [39]. Tissue engineering has revolutionized the field of dentistry by providing new solutions for the repair, regeneration, and restoration of damaged or missing dental tissues. Among the critical components in tissue engineering, scaffolds play a vital role in providing structural support and guiding cellular processes to promote tissue regeneration. In recent years,

natural and synthetic polymeric scaffolds have emerged as promising candidates for dental tissue engineering applications, owing to their unique properties and biocompatibility [32].

Natural polymers, such as collagen, fibrinogen, keratin, and chitosan, have been extensively studied as scaffold materials for dental tissue engineering. These polymers possess excellent biocompatibility and mimic the extracellular matrix (ECM) of dental tissues, promoting cell attachment, proliferation, and differentiation. For example, collagen scaffolds have been used to regenerate dental pulp tissue, whereas chitosan scaffolds have been used to regenerate periodontal tissue [32-33]. Additionally, synthetic polymers such as poly (lactic-co-glycolic acid) (PLGA), poly(caprolactone) (PCL), and polyethylene glycol (PEG) have shown great potential for dental tissue engineering applications. These polymers offer tunable mechanical and degradation properties, allowing the development of scaffolds with optimal properties for specific dental tissue engineering applications [34].

In addition to their biocompatibility, both natural and synthetic polymeric scaffolds can be fabricated using various techniques, including electrospinning, freeze-drying, and 3D printing, to create scaffolds with controlled pore sizes, shapes, and distributions [35]. Such techniques have been employed to develop scaffolds for a wide range of dental tissues including enamel, dentin, pulp, and periodontal tissues [35-36].

Despite considerable progress in the development of natural and synthetic polymeric dental tissue scaffolds, several challenges remain. A critical challenge is the ability to create scaffolds that can support the regeneration of complex dental tissues with multiple cell types and intricate structures. Additionally, issues such as biodegradation rate and inflammatory response must be considered when designing scaffolds for dental tissue engineering [37].

In conclusion, natural and synthetic polymeric scaffolds offer great promise for dental tissue-engineering applications. By providing a biocompatible ECM-like environment for cells, these scaffolds can support the regeneration of a wide range of dental tissues. Ongoing research on scaffold design and fabrication techniques will continue to drive innovation in the field of dental tissue engineering.

2.1.2.1. Poly (ε-caprolactone) (PCL)

PCL has garnered significant attention because of its biodegradable nature, favorable compatibility with other polymers, and ability to stick at low temperatures. This aliphatic polyester is created by the ring-opening polymerization of ε-caprolactone and is semi-crystalline with a high elongation, melting point of 67 °C, and glass transition temperature of -65 to -60℃. PCL can be blended with plasticizers such (polyethylene glycol) and glycerol when used in composites [40]. It has a density of 1.145 g/cm3 and a crystallinity degree ranging from 45 to 67%, and its physical, mechanical, and thermal properties, as well as its degradation rate, are significantly affected by variations in its molar mass and degree of crystallinity. PCL is widely used in scaffold production for tissue engineering, where it can control the pore shape, size, distribution, and interconnectivity to replicate the natural extracellular matrix of the tissue being replaced or regenerated. Its major use is in drug carrier production, where it forms structures that allow for high drug permeation. PCL degradation in vivo does not lead to microenvironmental acidification [41-42]. Nonetheless, PCL is hydrophobic and lacks the functional groups that limit cell attachment and proliferation [43].

2.1.2.2. Diethyl Allyl Phosphate (DAP)

Diethyl allyl phosphate, whose chemical formula is shown in (**Figure 2.1.)** is a colorless, liquid organic compound that is commonly used as a plasticizer in various industrial applications, including the manufacture of adhesives, coatings, and synthetic resins. Some of its specific specifications include its boiling point of 220°C (428°F), flash point of 60°C (140°F), and solubility in water [44]. In cell culture, DAP has been shown to enhance cell adhesion, proliferation, and differentiation [45]. This makes it a promising option for promoting tissue regeneration and repair. Additionally, DAP has been used to modify the properties of hydrogels and nanofibers, which are commonly used as scaffolds in tissue engineering applications. DAP has been shown to improve the mechanical properties of hydrogels and nanofibers, including their tensile strength and modulus. This makes them more suitable for tissue engineering applications. However, it is important to note that the use of DAP in cell culture and tissue engineering is still in its early stages, and more research is needed to fully

understand its potential benefits and limitations [46]. The potential toxicity of DAP and its impact on cell behavior in vivo must be carefully considered before its widespread use in these applications. DAP has been explored for its potential applications in cell culture and tissue engineering. Cell culture is a method of growing cells in a controlled environment, while dental tissue engineering is a rapidly growing field that aims to develop functional replacement tissues for damaged or diseased tissues using biological and synthetic materials [47].

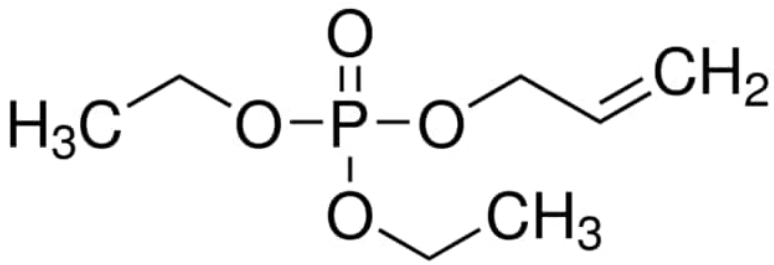

Figure 2.1. Diethyl Allyl Phosphate (DAP) monomer chemical structure.

2.2. Electrospinning Process

Electrospinning is a versatile spinning process that is used for fiber formation. It requires a DC voltage source in the range of several tens of kV in order to produce electrostatic forces. The process is mainly based on the principle that strong electrical repulsive forces exist between similar charges in the liquid droplet. The electrostatic force is a phenomenon that is observed due to the electrostatic repulsions between similar charges in the liquid. It affects the liquid and causes the shape of the droplet to change from a rounded meniscus to the Taylor cone. At this critical point, the applied electric field eventually becomes more prominent. It also overcomes the surface tension of the liquid, leading to a jet of the solution ejected from the tip of the Taylor cone. Since the jet travels through the air, the flow changes from ohmic to convective because the charges go towards the surface of the fiber. The electrospinning process produces an unstable jet of solvent which emerges between the tip and the collector, leading to the evaporation of the solvent. By leaving the solid fiber behind, the process results in a continuous fiber formation with diameters ranging from tens of nanometers to several micrometers [48-49]. The process should be carried out under properly

ventilated conditions to avoid unpleasant or even harmful emissions of some polymers or solvent vapors [50].

2.2.1. Parameters Affecting the Process

There are various parameters that affect the electrospinning process. These parameters typically fall into two main categories; The first concerns solution parameters such as viscosity, conductivity, surface tension. The second concerns process parameters such as applied electric field, capillary-collector spacing, and feed rate. Each of these groups deals with parameters that can lead to different fiber morphologies and diameters. As a result, one can control the desired fiber formation by appropriate manipulation of these parameters.

2.2.1.1. Solution Parameters

The ability of a polymer solution to be spun into fibers is dependent on its concentration. If the concentration is too low, the surface tension will cause the formation of beads instead of fibers. On the other hand, if the concentration is too high, the high viscosity will prevent fiber formation. However, within a specific optimal concentration range, the fiber length and diameter will be proportional to the concentration [51].

- **Molecular Weight**

A polymer's molecular weight is a reflection of chain interactions like Van der Waals attractions and entanglements. Thus, molecular weight-related characteristics like viscosity, surface tension, conductivity, and dielectric strength are addressed by the rheological and electrical properties of electrospinning solutions [52]. When compared to the same polymers with a lower molecular weight, a high molecular weight polymer's viscosity in a solution actually has a higher viscosity [53-54].

- **Conductivity**

One or more factors affecting conductivity in an electrospinning solution include the type of solvent, the polymer, or charged ions in the solution. Solutions that are highly conductive have greater charge and carrying capacities than those that are low in conductivity.

For solutions that produced enough elongation and bead formation, they are subjected to higher tensile forces in an electric field. Increased tensile forces also cause a reduction in fiber diameter. It is connected to the solution conductivity's cube root, as Baumgarten illustrated [55]. With a few notable exceptions, the majority of polymers are conductive, so different solvents, solution concentrations, and the addition of ionic salts were used in the studies to control the effect of conductivity.

- **Viscosity**

The critical factor in determining fiber morphology in electrospinning is solution viscosity. It has been established that smooth and continuous fibers cannot be produced with low viscosity, leading to the formation of bead-like fibers. On the other hand, excessively high viscosity can result in the hard ejection of jets from the solution, making it necessary to have an optimal viscosity for the process to be successful. The solution viscosity can be adjusted by changing the polymer concentration, enabling the production of different fiber morphologies. It is important to keep in mind that viscosity, polymer concentration, and polymeric molecular weight are interrelated [56].

2.2.1.2. Process Parameters

- **Applied Electric Field**

The applied voltage plays a crucial role in the electrospinning process as it is necessary to generate an electric field strong enough to overcome the surface tension of the liquid and facilitate fiber formation. The impact of the applied voltage on fiber diameter is a matter of debate among scientists. Some researchers claim that an increase in mass flow rate, due to the electrostatic force, results in larger fiber diameters, and that the applied voltage has no effect on fiber diameter [57]. On the other hand, other authors suggest that higher voltage levels cause the solution to stretch, increasing the columbic forces in the jet and leading to smaller fiber diameters [58]. There is conflicting views on the relationship between voltage and bead formation. Studies have explored bead formation under both high and low voltage conditions, with slower feed rates leading to bead formation at low voltages and larger amounts of solution ejected causing bead formation at high voltages.

- **Capillary – Collector Distance**

The another factor is the distance between the collector and the capillary. Bead formation and fiber diameter are both affected by it. If a beaded morphology is to be expected, the solvent must evaporate at a minimum distance [59]. However, the longer the solvent evaporation period is, the smaller the fiber diameter becomes. However, Pham et al. [60] found that the effect of distance varies depending on the polymer utilized. Demonstrated that shorter distances have resulted in smaller fibers for polysulfone.

- **Feeding Rate**

In the electrospinning process, it is essential to regulate the flow rate of the solution so that the Taylor cone remains visible throughout. However, reducing the flow rate can result in finer fibers by allowing sufficient time for solvent evaporation [60]. The most significant impact of the flow rate is the formation of porous structures on the fibers. Research indicates that an increase in flow rate leads to larger pore size, which is probably related to the amount of solvent present during the formation of the jet [61].

- **Humidity**

The level of humidity can have an impact on the evaporation rate of the solvent and the porosity of fibers. As humidity increases, the porosity of fibers also increases, which facilitates the release of the solution from the needle tip. On the other hand, if humidity is low, it may cause the solution in the needle tip to dry out and block the tip [74].

- **Temperature**

Temperature fluctuations can affect the viscosity of the solution and the evaporation rate of the solvent. As the temperature increases, the kinetic energy of particles also increases, leading to a decrease in viscosity. This in turn causes the fibers to stretch [75].

2.2.1.3. Types of Electrospinning

The most basic electrospinning setup is either horizontal or vertical, with a single spinneret ejecting a single type of liquid. However, more advanced setups have been developed to produce more intricate nanofibrous structures in a controlled and efficient

manner, due to the growing interest in this technology among research groups. One such setup is the sequential spinning of two different solvents to create a multilayered fiber mesh or a dual spinneret system that ejects two solvents simultaneously onto an alternating collector. Another setup is the direct integration of cells into the fiber mesh using a dual spinneret system with a perpendicular capillary configuration, where fiber and cells are ejected simultaneously onto a rotating mandrel moving along a linear stage [62]. Additionally, it is possible to produce composite and/or hybrid fibers, such as **core-shell type** single fibers, through the **coaxial spinning of two different polymer solutions from a single modified capillary tip** [63]. These different electrospinning setups are depicted in (**Figure 2.2.** and **Figure 2.3**.). In conclusion, the structural and topological properties of electrospun scaffolds can be altered through different experimental setups, such as the number and design of spinnerets and the design of the grounded collector plate, which can be stationary, rotating, and/or alternating (**Figure 2.4** and **Figure 2.5**.)

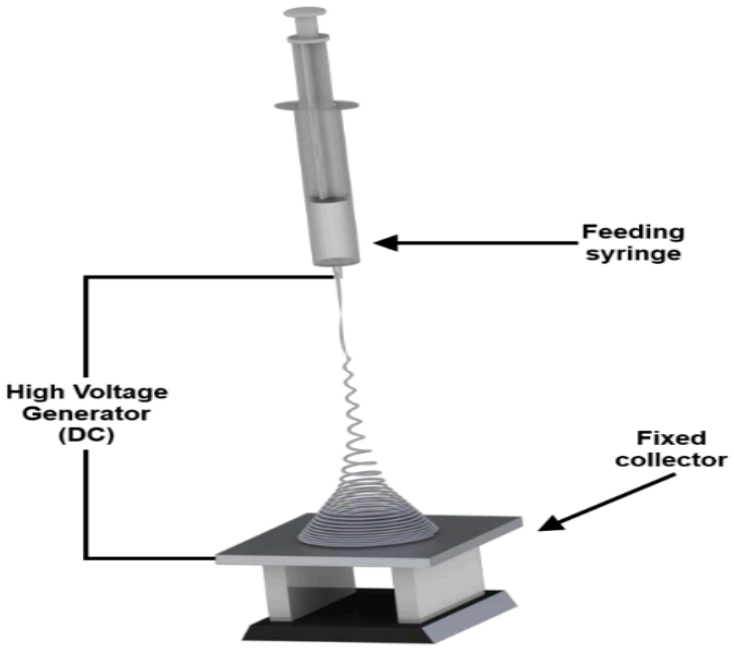

Figure 2.2. Vertical electrospinning setup.

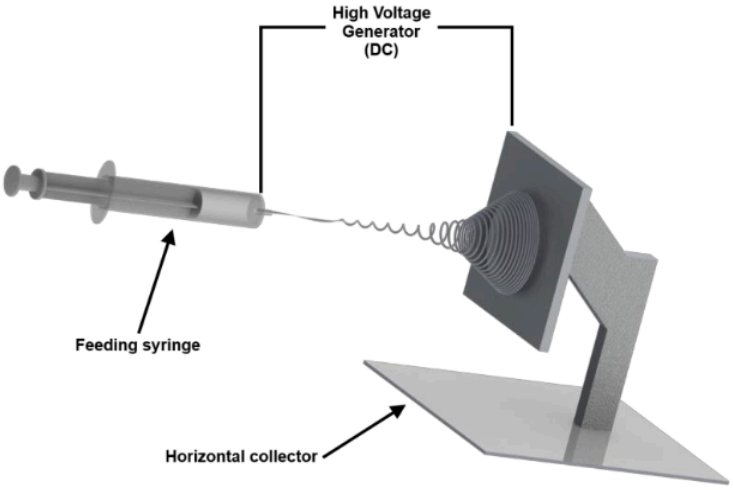

Figure 2.3. Horizontal electrospinning setup.

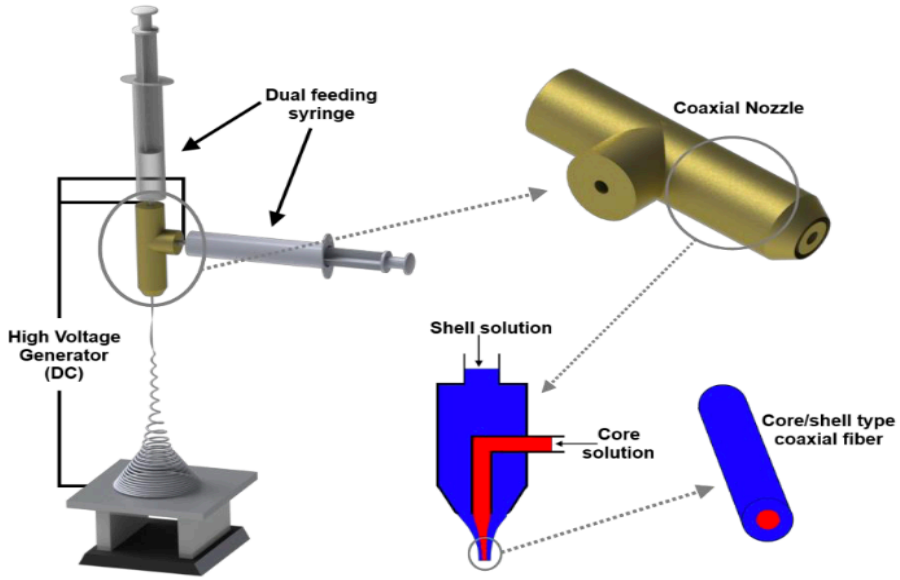

Figure 2.4. A modified nozzle configuration for coaxial electrospinning, where one syringe delivers the core solution and the other provides the shell solution, producing single two-component fibers.

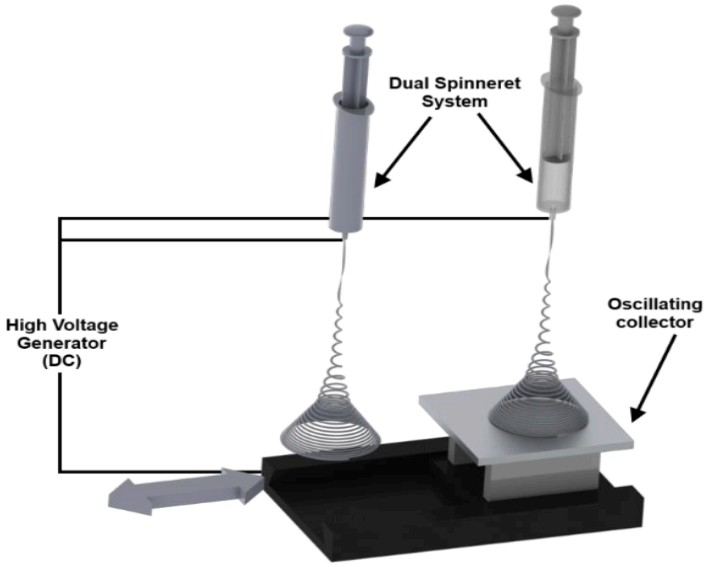

Figure 2.5. A vertical electrospinning setup featuring two distinct syringes and a horizontal oscillating collector, which can be used for either sequential spinning to produce a multilayered mesh or dual spinning to create a single layer of blended fibers.

2.2.1.4. Applications

The electrospinning process has gained significant attention in recent years due to its various advantages, including a high surface area to volume ratio, high porosity, and some mechanical properties. The desired morphological and mechanical properties for a specific application can be achieved by manipulating the solution and process parameters. There have been numerous studies of electrospinning for various applications, each taking advantage of the unique properties of the process and resulting structure. For example, in dental tissue engineering, the fibrous structure provides mechanical support and anchorage for cells, while also allowing for the integration of various materials and therapeutic dental agents. The high surface area to volume ratio and adjustable porosity of the electrospun structures are beneficial in filtration applications, while the selective permeability makes it useful in wound dressing and wound healing usage. In drug delivery, the versatility of electrospinning allows for the creation of a controllable drug delivery system through mechanisms such as diffusion, degradation, or swelling, using a wide range of materials and therapeutic agents. Despite the different properties required for different applications, every area can benefit from the ease of use of the electrospinning process.

2.3. Dental Wound Healing Process

The wound healing process is a complex and well-coordinated series of events that follow a specific order. For proper healing, it is essential to have functioning hemostatic and inflammatory systems, as well as the migration and proliferation of mesenchymal cells at the site of the injury. The formation of new tissue relies on angiogenesis, epithelialization, and the synthesis, binding, and alignment of collagen, which contribute to wound contraction [77]. Wound healing also includes both regeneration (**replacing damaged tissues with identical cells**) and fibrosis (**substituting damaged tissues with connective tissue**).

2.3.1. Dental Wound Healing Progression

The wound healing process begins with the creation of a blood clot that seals the wound. To halt bleeding, vasoconstriction takes place, followed by platelet activation. Platelets have various crucial functions in a wound, such as managing primary hemostasis during aggregation and secondary hemostasis during coagulation. They generate biologically active substances like vasoactive mediators, chemotactic factors, proteases, cytokines, and growth factors [78]. Cytokines emit chemotactic signals to inflammatory cells and local cell populations. The fibrin-fibronectin clot formed in secondary hemostasis acts as a temporary scaffold for epithelial cells and fibroblasts to migrate into the wound. Thrombin is activated upon clot formation to prevent excessive blood clotting [79]. During the third hemostatic phase, activation of the fibrinolytic system leads to fibrin breakdown. The peptides released during this phase induce chemotaxis and enhance capillary permeability.

Cytokines initiate an inflammatory response that helps clear debris, damaged or dead tissues, and microorganisms [80]. Blood vessels near the wound exhibit dilation, increased capillary permeability accompanied by plasma leakage, and reduced blood flow. Leukocytes are drawn to the wound center, which quickly becomes filled with granulocytes and macrophages. Initially, neutrophilic granulocytes protect against bacterial invasion, while macrophages become the predominant cells after a few days. Macrophages also significantly contribute to collagen synthesis and the formation of endothelial cells and fibroblasts, effectively driving the wound healing process [81].

Both granulocytes and macrophages exhibit anaerobic metabolism, generate collagenase, consume bacterial debris, and produce lactate, which lowers tissue pH [82]. According to hemostasis, this process requires regulation, with acceleration, amplification, and downregulation being crucial for normal wound healing. Prostaglandins and leukotrienes serve as pro-inflammatory mediators, while lipoxins, resolvins, and protectins suppress inflammatory reactions [80]

The inflammatory phase is succeeded by the formation of granulation tissue, re-epithelialization, and development of a connective tissue matrix. Granulation tissue consists of a dense population of macrophages, fibroblasts, capillary networks, fibronectin, hyaluronic acid, and endothelial cells. Macrophages, fibroblasts, and endothelial cells are interdependent during the formation of granulation tissue [83]. Hypoxia serves as a critical stimulus for neovascularization during this stage [84-85]. Fluid continues to seep from the wound until the basal membrane forms. At this point, fibroblasts are attracted from the wound edges, and circulating fibrocytes and mesenchymal progenitor cells migrate to the immature connective tissue matrix [87].

Re-epithelialization begins at the wound edge, where epithelial cells detach from their hemi-desmosomal connections and migrate through the temporary fibrin-fibronectin matrix within the wound until they meet similar cells [87]. This targeted migration and proliferation through a loose underlying network demands an effective, balanced, and enzyme-assisted process of "cutting and pasting" [86-87]. When the epithelial cells from both wound edges come into direct contact, it is called healing by primary intention. In contrast, healing by secondary intention takes place when migrating cells connect after some time, either through granulation tissue or not [83]. Open wounds heal more slowly due to delayed epithelial closure and an increased rate of granulation tissue formation [83-88]. The initial fibronectin connective tissue is loose and is gradually replaced by larger and stronger collagen bundles, which protect the wound from traction and pressure damage. ECM formation starts at the wound edge and gradually advances towards the wound's center from the core or both of them. This process is akin to matrix maturation, as both begin at the edge and progress gradually toward the wound center. During maturation, the formation of new blood vessels diminishes [82-87].

The final stage of wound healing, known as the contraction phase, commences after adequate collagen has formed within the granulation tissue. During this phase, the distance between wound edges narrows, reducing the wound surface and hastening closure. This final process takes place due to the differentiation of fibroblasts and other progenitor cells into myofibroblasts, which possess an actin-rich cytoskeleton that enables matrix constriction. Wound contraction is followed by the remodeling process, where matrix production ceases, fibroblasts degrade, and myofibroblasts undergo apoptosis [82-87]. The ultimate outcome of wound healing can vary from a clinically healed wound with no scarring and histologically normal connective tissue beneath the epithelial cells to severe trismus resulting from fibrosis.

2.3.2. Periodontal Wound Healing

The healing process following a tooth extraction adheres to the same pattern, with the addition of bone healing. Shortly after the tooth is removed (**Figure 2.6)**, blood clotting seals the alveoli. Re-epithelialization system begins 24 hours after tooth extraction. Within a week, the blood clot is replaced by granulation tissue. The around 8-week healing process, the extraction cavity is filled with bone [84-85]. **Bone remodeling persists for six months post-extraction, accompanied by a loss of alveolar width and length due to resorption and remodeling** [84]. The extent of bone loss varies among individuals, depending on factors such as location, adjacent teeth presence, treatment protocol, smoking habits, and the use of membranes and bone substitutes. A review on the effects of plasma concentrates revealed a reduction in post surgical pain and discomfort but no enhancement or increase in hard tissue regeneration [85].

Wound healing after periodontal surgery poses a significant risk of interdental papilla degradation, leading to the appearance of black triangles. Precise incisions and flaps are crucial for minimizing retraction, and maintaining good oral hygiene is essential to prevent inflammation [85].

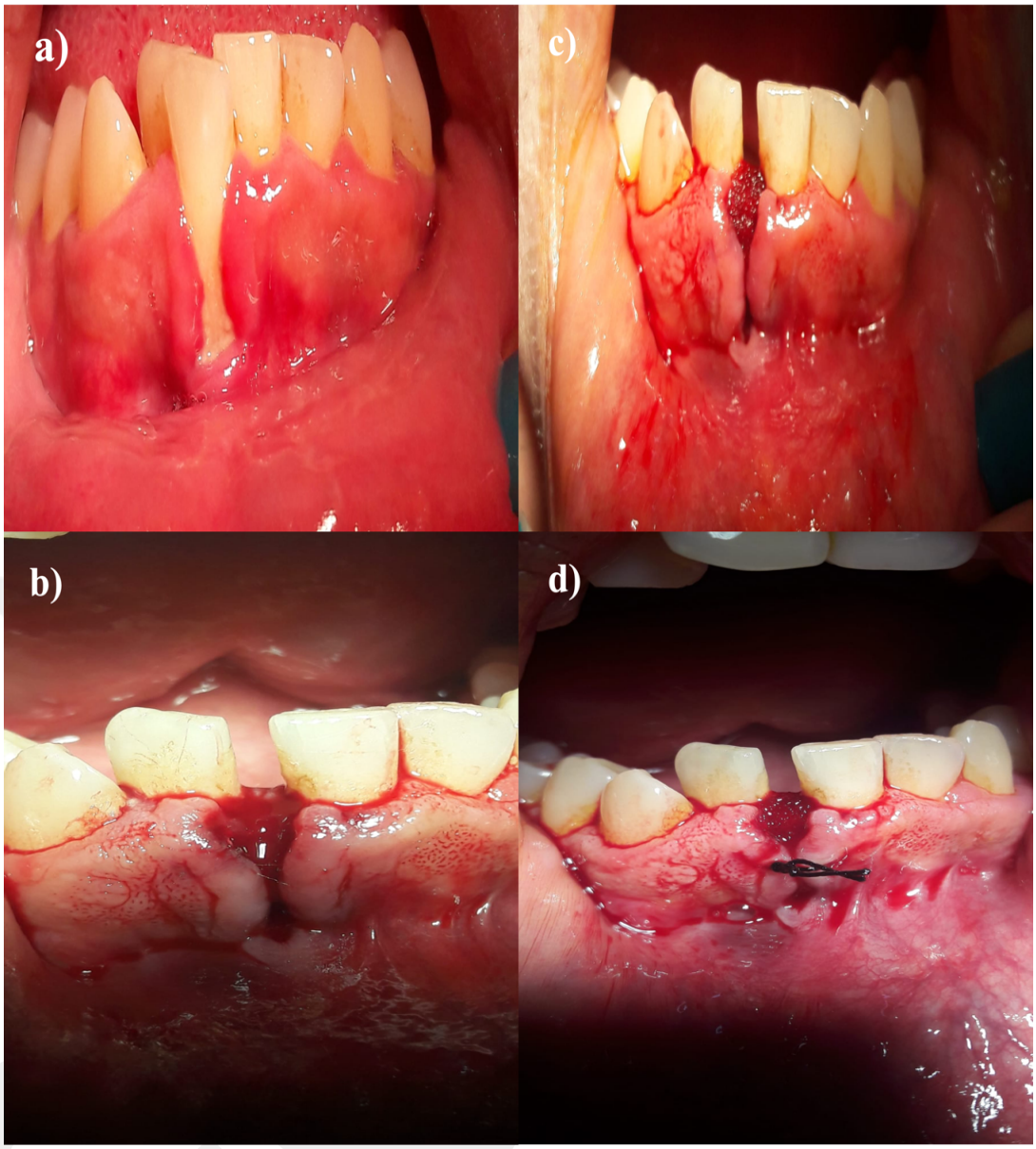

Figure 2.6. Tooth extraction steps; a) Mandibular Right Central Incisor tooth planned to be extracted, b) open wound site after tooth extraction operation., c) Sponge placed inside the tooth extraction wound to help absorb bleeding, d) Suturing the wound site with suture.

2.3.3. Dental Pulp Healing

The survival of the injured odontoblast layer and the preservation of the blood vessels at the apex are critical for the repair of dental pulp. When the odontoblast layer is sufficiently intact, it can induce reactive dentin production. Even if only the surface of the pulp is injured, an inflammatory reaction may draw cell lines or progenitor cells to the wound site, where they can develop into odontoblast-like cells and create

reparative dentin or osteodentin. Therefore, Chronic inflammation in the tooth pulp might result in inflammatory changes [86].

2.3.4. Dental Wound Dressing

In a dental setting, wound dressings are used to cover and protect oral wounds that occur as a result of dental procedures, such as extractions, biopsies, or surgical procedures. They are also used to treat oral injuries that may occur due to accidental trauma, such as lacerations or cuts to the gums, lips, or cheek. The main function of a dental wound dressing is to provide a physical barrier to prevent further injury, reduce pain and discomfort, and promote healing [64].

There are various types of dental wound dressings available, each with its own set of properties and benefits. For example, some dental wound dressings are designed to be highly absorbent, helping to manage excess fluid and promote a clean, dry wound environment. Others are designed to be occlusive, meaning that they create a barrier to prevent the entry of bacteria and other potentially harmful agents into the wound. Some dental wound dressings also contain antimicrobial agents, such as silver or honey, to help prevent infection and promote healing [65-66].

The choice of dental wound dressing depends on various factors, including the location and size of the wound, the type of procedure that was performed, and the patient's overall health and medical history. For example, in the case of a patient with a history of allergies or sensitivity to certain materials, a dentist may choose a dressing made from a hypoallergenic material. Similarly, in the case of a large, deep wound, a dentist may choose a dressing with a high level of absorbency to help manage excess fluid and promote healing [67].

In conclusion, dental wound dressings play an important role in the management of oral wounds and injuries. By providing a physical barrier, reducing pain and discomfort, and promoting healing, they can help to ensure a positive outcome for patients following dental procedures or accidents [68-75].

2.4. Dielectric Barrier Discharge (DBD) Plasma

Dielectric Barrier Discharge (DBD) plasma is a type of non-thermal plasma generated by applying a high voltage across two electrodes separated by a dielectric material.

The high electric field creates a discharge, which ionizes the gas and produces a plasma. This type of plasma is often referred to as "cold" plasma because the temperatures of the ions and electrons are much lower than in thermal plasmas [69].

DBD plasma has a wide range of applications, including surface modification, material synthesis, and environmental remediation. In surface modification, DBD plasma is used to change the surface properties of materials, such as wettability, adhesion, and biocompatibility. This can be accomplished by adding or removing functional groups from the surface of the material or by changing its surface energy [70].

DBD plasma is also used in material synthesis to produce nanomaterials, such as nanoparticles and nanofibers, by breaking down precursors in the plasma. In environmental remediation, DBD plasma is used to destroy pollutants and pathogens in air and water [69-70].

Overall, DBD plasma is a versatile technology with many potential applications in various fields due to its ability to modify surfaces and produce nanomaterials in a controlled and reproducible manner.

Dielectric Barrier Discharge (DBD) plasma can modify the surface topography of PCL (Polycaprolactone) nanofibers. The modification occurs due to the interaction of plasma species with the surface of the PCL nanofibers. The effect of plasma on the PCL nanofibers depends on several parameters, such as the plasma gas composition, plasma power, and treatment time [71].

DBD plasma treatment can lead to the removal of the PCL nanofiber's surface layer, resulting in the exposure of the underlying fibers. This process can alter the surface topography of the PCL nanofibers, making them more rough or smooth and textured. The surface roughness or smoothness and texture can be controlled by adjusting the plasma parameters [72].

Moreover, DBD plasma treatment can also introduce functional groups, such as -OH, -COOH, and $-NH_2$, on the surface of PCL nanofibers. These functional groups can improve the surface energy and wettability of the PCL nanofibers, which is beneficial for applications such as tissue engineering and drug delivery [73].

DBD plasma treatment can modify the topography of PCL nanofibers by changing their surface roughness and introducing functional groups, which can improve their surface properties and enhance their performance for various applications.

2.4.1. Dielectric Barrier Discharge (DBD) Plasma Applications

2.4.1.1. Surface Modification

DBD plasma is used to modify the surface properties of materials, such as wettability, adhesion, and biocompatibility. This can be accomplished by adding or removing functional groups from the surface of the material or by changing its surface energy. For example, DBD plasma has been used to modify the surface of polymers, such as polycaprolactone (PCL), to improve cell adhesion and proliferation. The plasma can also be used to modify the surface of metals, ceramics, and glass to improve their wettability and biocompatibility.

2.4.1.2. Material Synthesis

DBD plasma is used to produce nanomaterials, such as nanoparticles and nanofibers, by breaking down precursors in the plasma. The plasma can also be used to synthesize new materials, such as coatings and films, by depositing reactive species from the plasma onto a substrate.

2.4.1.3.Environmental Remediation

DBD plasma is used to destroy pollutants and pathogens in air and water. For example, DBD plasma has been used to remove volatile organic compounds (VOC's) from air and to decontaminate water by breaking down pathogens and chemicals.

2.4.1.4. Food and Agriculture

DBD plasma is used to decontaminate food and improve the shelf life and quality of agricultural products. For example, DBD plasma has been used to remove bacteria and other contaminants from fruits and vegetables, and to improve the preservation of food products.

2.4.1.5. Medical and Biomedical Applications

DBD plasma is used for wound healing and tissue engineering, as well as for the sterilization of medical and dental instruments. For example, DBD plasma has been

used to promote cell proliferation and growth, and to sterilize medical devices and surfaces.

2.4.1.6. Energy and Fuel Technology

DBD plasma is used for the production of hydrogen fuel and the synthesis of fuels from biomass. For example, DBD plasma has been used to produce hydrogen from water and to convert biomass into biofuels.

CHAPTER 3

Experimental Study

3.1. Materials

Sigma-Aldrich supplied PCL (Poly (ε-caprolactone) (MW=80,000 g/mol, linear). Dichloromethane and chloroform solutions were used in the core-shell electrospinning process for the formation of a PCL/PCL structure with a core-shell morphology, while methanol was added to the solutions to enhance electrical conductivity and used as a solvent. Interlab supplied the glass petri dishes required for samples carrier (Ankara, Turkey). ATCC CCL-1 L929 mouse fibroblast cells were graciously provided by Kirikkale University's Department of Bioengineering for cell culture investigations (Kirikkale, Turkey). Amresco provided DMEM (Dulbecco's Modified Eagle Medium), FBS (fetal bovine serum), L-glutamine, penicillin/streptomycin, BSA (bovine serum albumin), and Phosphate buffer saline (PBS) tablets (Solon, USA). Sigma-Aldrich (St. Louis, USA) provided ethanol (99% purity, vol/vol.), MTT powder (3-(4,5-dimethyl-2-thiazol)-2,5-diphenyl-2H-tetrazolium bromide), Trypsin/EDTA solution at 0.25% (w/v.), Triton X-100, glutaraldehyde, dimethylsulfoxide (DMSO), hexamethyldisilazane (HM (St. Louis, USA). Acridine Orange dye (AO) and Propidium Iodide dye (PI) were also purchased from Sigma-Aldrich (St. Louis, USA). Diethyl Allyl Phosphate (DAP) was purchased from Sigma-Aldrich (St. Louis, USA).

3.2. Preparations of the Samples

3.2.1. Production of Core-Shell PCL/PCL Scaffolds

Coaxially electrospinning processes were used to create the 3D core-shell PCL/PCL scaffolds. For sample 1, core PCL (2 w/w%) was dissolved in dichloromethane by magnetic stirring at room temperature for 2 hours. The solutions were drawn into the syringe in 5 mL increments. Shell PCL (2 w/w%) was dissolved in chlorofom by magnetic stirring at room temperature for 2 hours. The liquids were drawn into the syringe in 5 mL volumes. Core PCL (2 w/w%) was dissolved in chloroform by magnetic stirring for 2 hours at room temperature in sample 2. The liquids were drawn into the syringe in 5 mL volumes. Shell, PCL (2 w/w%) was magnetically stirred for

2 hours at room temperature in dichloromethane. The syringe was filled with the solutions in a 5 mL volume. The samples were put in petri plates for drying after two independent coaxial electrospinning procedures. To remove any remaining solvents, they were wrapped with aluminum foil, pinned, and left at room temperature for three days. The materials were kept in desiccators throughout this time until the subsequent experiments.

3.2.2. Preparation of the Coaxial Electrospinning Solutions

Electrospun core-shell PCL solution conditions that were previously used in our lab. At the beginning, for sample 1, PCL pellets were precisely weighted (2% (wt/vol.)) and dissolved in a mixture of dichloromethane and methanol with a volume ratio of 5:2 for the shell structure and PCL pellets were precisely weighted (2% (wt/vol.)) and dissolved in a mixture of chloroform and methanol with a volume ratio of 3:2 for the core structure.

For sample 2, PCL pellets were precisely weighted (2% (wt/vol.)) and dissolved in a chloroform and methanol combination with a 3:2 volume ratio for the shell structure and a dichloromethane and methanol mixture with a 5:2 volume ratio for the core structure. Each solution was mixed for 2 hours with a magnetic stirrer until clear homogenized solutions were seen. Lastly, the PCL solutions from each sample were held at room temperature for 10 minutes to remove any air bubbles.

3.2.3. Optimization and Determination of Coaxial Electrospinning Process

To prepare electrospun PCL and core-shell scaffolds, the PCL/PCL solution and electrospinning process parameters were optimized. The sample groups with the production stages were divided into two groups based on core-shell properties. Sample 1 was produced using DCM in the core and chloroform in the shell, while sample 2 was produced using chloroform in the core and DCM in the shell. In this production process, the viscosities of the solvents were examined. Optimization conditions were given in the following below (**Tables 3.1-3.7**.).

Electrospinning process parameters, such as applied voltage, fleeding rate, and distance between needle-collectors, were optimized to produce electrospun pure core PCL, pure shell PCL, and core/shell PCL/PCL (2wt% and 6wt%). For pure PCL, the

same electrospinning parameters were used as those determined in our previous study [88]. Hence, a coaxial nozzle electrospinning apparatus was utilized, and optimization was performed. To optimize the electrospinning process, a wide range of electrospinning parameter experiments was carried out, as shown in the tables below.

Table 3.1. Structure of 2% (w/v) PCL polymer. Effects of Chloroform/Methanol solvents in electrospinning studies to produce Shell structure of 2% (w/v) PCL polymer.

Sample	Experiment No	Needle-Collector Distance (cm)	Feeding Rate (μL/Min)	Voltage (kV)	Observation
2 wt% PCL	1	10	2	15	Not-Spinned
	2	10	5	15	Not-Spinned
	3	10	10	15	Not-Spinned
	4	10	2	20	Not-Spinned
	5	**10**	**5**	**20**	**Spinned**
	6	10	10	20	Not-Spinned
	7	15	2	15	Not-Spinned
	8	15	5	15	Not-Spinned
	9	15	10	15	Not-Spinned
	10	15	5	20	Not-Spinned

Table 3.2. Effects of Chloroform/Methanol solvents in electrospinning studies to produce Shell structure of 6% (w/v) PCL polymer.

Sample	Experiment No	Needle-Collector Distance (cm)	Feeding Rate (μL/Min)	Voltage (kV)	Observation
	1	10	2	15	Not-Spinned
	2	10	5	15	Not-Spinned
	3	10	10	15	Not-Spinned

6 wt% PCL	4	15	2	20	Not-Spinned
	5	15	5	20	Not-Spinned
	6	**15**	**10**	**20**	**Spinned**
	7	15	2	20	Not-Spinned
	8	20	5	20	Not-Spinned
	9	20	10	20	Not-Spinned
	10	20	2	20	Not-Spinned

Table 3.3. Effects of Dichloromethane/Methanol solvents in electrospinning studies to produce Core structure of 2% (w/v) PCL polymer.

Sample	**Experiment No**	**Needle-Collector Distance (cm)**	**Feeding Rate (μL/Min)**	**Voltage (kV)**	**Observation**
2 wt% PCL	1	10	2	15	Not-Spinned
	2	10	5	15	Not-Spinned
	3	10	10	15	Not-Spinned
	4	10	15	15	Not-Spinned
	5	**10**	**20**	**15**	**Spinned**
	6	15	5	15	Not-Spinned
	7	15	10	20	Not-Spinned
	8	15	20	15	Not-Spinned
	9	20	10	15	Not-Spinned
	10	20	20	20	Not-Spinned

Table 3.4. Effects of Dichloromethane/Methanol solvents in electrospinning studies to produce Core structure of 6% (w/v) PCL polymer.

Sample	Experiment No	Needle-Collector Distance (cm)	Feeding Rate (µL/Min)	Voltage (kV)	Obsevation
6 wt% PCL	**1**	**10**	**2**	**15**	**Spinned**
	2	10	5	15	Not-Spinned
	3	10	10	15	Not-Spinned
	4	15	2	20	Not-Spinned
	5	15	5	20	Not-Spinned
	6	15	10	20	Not-Spinned
	7	20	2	15	Not-Spinned
	8	20	5	15	Not-Spinned
	9	20	10	20	Not-Spinned
	10	20	20	20	Not-Spinned

Table 3.5. Core/Shell (Core: DCM, Shell: Chlorofom) structure of 2 wt% PCL/PCL electrospun fiber production parameters for Sample 1.

Sample 1	Experiment No	Needle-Collector Distance (cm)	Feeding Rate (µL/Min) (DCM)	Feeding Rate (µL/Min) (Chloroform)	Voltage (kV)	Obsevation
2 wt% PCL	1	10	10	2	15	Not-Spinned
	2	10	5	5	15	Not-Spinned
	3	10	2	10	15	Not-Spinned
	4	**10**	**10**	**2**	**20**	**Spinned**
	5	10	5	5	20	Not-Spinned
	6	10	2	10	20	Not -Spinned
	7	15	10	2	15	Not-Spinned
	8	15	5	5	15	Not-Spinned
	9	15	2	10	15	Not-Spinned

	10	15	10	2	20	Not-Spinned
	11	15	5	5	20	Not-Spinned
	12	15	2	10	20	Not-Spinned
	13	20	10	2	15	Not-Spinned
	14	20	5	5	15	Not-Spinned
	15	20	2	10	15	Not-Spinned
	16	20	10	2	20	Not-Spinned
	17	20	5	5	20	Not-Spinned
	18	20	2	10	20	Not-Spinned

Table 3.6. Core/Shell (Core: Chloroform, Shell: DCM) structure of 2 wt% PCL/PCL electrospun fiber production parameters for Sample 2.

Sample 2	**Experiment No**	**Needle-Collector Distance (cm)**	**Feeding Rate (µL/Min) (DCM)**	**Feeding Rate (µL/Min) (Chloroform)**	**Voltage (kV)**	**Obsevation**
2 wt% PCL	1	10	10	2	15	Not-Spinned
	2	10	5	5	15	Not-Spinned
	3	10	2	10	15	Not-Spinned
	4	10	10	2	20	Not-Spinned
	5	10	5	5	20	Not-Spinned
	6	10	2	10	20	Not-Spinned
	7	15	10	2	15	Not-Spinned
	8	15	5	5	15	Not-Spinned
	9	15	2	10	15	Not-Spinned
	10	15	10	2	20	Not-Spinned
	11	15	5	5	20	Not-Spinned
	12	**15**	**2**	**10**	**20**	**Spinned**
	13	20	10	2	15	Not-Spinned
	14	20	5	5	15	Not-Spinned
	15	20	2	10	15	Not-Spinned

	16	20	10	2	20	Not-Spinned
	17	20	5	5	20	Not-Spinned
	18	20	2	10	20	Not-Spinned

Table 3.7. Core-Shell structures production samples chemical values.

Sample 1	Sample Values (mL)
2 wt% PCL (For Core Structure)	• 5 mL Dichloromethane • 2 mL Methanol
2 wt% PCL (For Shell Structure)	• 3 mL Chloroform • 2 mL Methanol

Sample 2	Sample Values (mL)
2 wt% PCL (For Core Structure)	• 3 mL Chloroform • 2 mL Methanol
2 wt% PCL (For Shell Structure)	• 5 mL Dichloromethane • 2 mL Methanol

3.3. Dielectric Barrier Discharge Plasma

The PCL/PCL samples produced as electrospun core-shell were cut into 5x3 dimensions and a total of 4 samples were prepared for each sample group. The samples were divided into sample group 1 and sample group 2. For the application of DBD plasma processing, three different samples were prepared, totaling 6 different samples, for both sample group 1 and sample group 2. The first samples of sample group 1 and sample group 2 were connected to an argon gas supply and 100 µL of Diethyl Allyl Phosphate (DAP) liquid was added and a 1 min DBD plasma processing was carried out to coat the surfaces with plasma and DAP. This process was applied to both sample groups and the remaining samples were coated with plasma and DAP for 3 and 5 minutes. The remaining samples which were electrospun core-shell PCL/PCL from the two sample groups were not subjected to surface coating with plasma and DAP.

3.4. Characterizations

3.4.1. Thickness Measurements

The thicknesses of electrospun core-shell PCL/PCL nanofibers, sample 1 group, and sample 2 group were measured with a micrometer (outside micrometer, 0-25 mm, USA), and average values were determined from 10 measurements of various samples from the same batch.

3.4.2. Contact Angle (CA) Measurements

Using the sessile drop water contact angle measurement technique, the contact angle values of electrospun untreated core-shell PCL/PCL nanofibers, sample 1 group and sample 2 group were measured as a function of surface tension of a variety of liquids (Phoenix 300, Surface Electro Optics, South Korea). For each test, three samples were used, and the average and standard deviation values for each sample were determined and compared to the reference surface wettability of commercial TCPS (Tissue Culture Polystyrene). Samples coated with DAP monomer using the DBD plasma method were exposed to DBD plasma treatment for 1, 3, 5, and 7 minutes. Then, the contact angle values of the samples, including electrospun PCL, electrospun core-shell PCL/PCL, and electrospun core-shell PCL/PCL produced by electrospinning, coated with DAP on surfaces treated with DBD plasma for 1, 3, 5, and 7 minutes, were examined.

3.4.3. Scanning Electron Microscopy (SEM) Analyses

Scanning Electron Microscope (Quanta 400F SEM from FEI in the USA) was utilized to inspect the obtained nanofibers to study their morphologies and core-shell structure. The samples were coated with gold before analysis. The fiber diameter and fiber pore size were calculated using ImageJ Launcher software based on SEM images. For the analysis, 10 images per sample were used, with at least 25 measurements taken, and the results were analyzed statistically using JStats 1.8 software.

3.4.4. Transmission Electron Microscopy (TEM) Analyses

TEM observations (FEI Tecnai G2 Spirit BioTwin CTEM, (USA)) were carried out to determine the electrospun untreated core-shell PCL/PCL structure, sample 1group and

sample 2 group of the electrospun core-shell nanofibers. The samples for TEM observation were prepared by placing a carbon-coated copper grid on the collector to directly deposit a very thin layer of electrospun fibers on the grid. Then, a copper grid containing fiber staining was used to obtain the TEM image by passing a beam of electrons through. The TEM analysis results were scaled using the ImageJ program and sorted alphabetically.

3.4.5. Mechanical Properties

The electrospun untreated core-shell PCL/PCL nanofibers, sample 1 groups and sample 2 groups were shaped into dog-bone form (40mm x 5mm) and their mechanical strength was measured using a Zwick/Roell universal tensile tester from Germany with a 100 N load cell. The testing took place at room temperature at a speed of 10 mm/min. For comparison, the mechanical properties were also assessed on electrospun PCL nanofibers.

3.4.6. Fourier Transform Infrared Spectroscopy (FTIR) Analyses

The chemical compositions of electrospun core-shell PCL/PCL, electrospun core-shell PCL/PCL 1 min DBD plasma with coated DAP, electrospun core-shell PCL/PCL 3 min DBD plasma with coated DAP, electrospun core-shell PCL/PCL 5 min DBD plasma with coated DAP nanofibers were determined with ATR-FTIR spectrometer (Bruker Vertex 70, Germany) with a scan resolution of 2 cm^{-1} in the range from 4000 to 450 cm^{-1} in order to obtain characteristic peaks of the materials and to observe interactions between electrospun core-shell PCL/PCL with 1,3 and 5 min DBD Plasma surface coated with DAP and electrospun PCL.

3.4.7. PBS Absorption and Shrinkage Tests

To determine the shrinkage and PBS absorption characteristics, rectangular-shaped pieces of the nanocomposite samples with dimensions of 10 mm x 5 mm were cut. These samples were then placed in bottles containing 20 mL of PBS (pH = 7.4) and incubated in vitro for 24 hours at 37.0℃. After the incubation period, the samples were removed from PBS, dried with a filter paper to remove excess water, and their weights

were measured. The water uptake of the samples in PBS was then calculated using the following formula;

$$A(\%) = \left(\frac{W_1 - W_0}{W_0} \right) x100$$

A (%) is the PBS absorption (%), W_0 (g) and W_1 (g) are the weights of the nanofibers before and after immersion in PBS medium for 24 h, respectively. For each group, three samples were taken after being incubated in PBS and dried in a vacuum oven for 12 hours to remove the excess water. The size of the dried samples was measured, the surface area was calculated, and compared to the initial area. The shrinkage percentage was then determined as the change in the surface area of the recovered Samples [88].

3.4.8. Water Vapor Transmission Rate (WVTR)

The water vapor transmission rate of the electrospun core-shell PCL/PCL nanofibers such as sample 1 and sample 2 were determined using the ASTM E96/E96M test method [89]. The results were obtained by measuring the weight loss of water in a bottle containing 10 mL of distilled water with a diameter of 50 mm. Samples with a thickness of 1.5 mm and dimensions of 50x50mm were tightly sealed on the top of the cylindrical cup. The sealed cups were then incubated at 37℃ for 24 hours. The WVTR was calculated using the following equation;

$$WVTR = \frac{W_0 - W_f}{A \times 24} x10^6 \ \text{g/m}^2\text{.day}$$

A is the mouth area of the bottle, W_0 (g) and W_f (g) are the weights of the bottle before and after the incubation operation for sample 2, respectively.

3.4.9. In Vitro Degradation

The degradation process of nanofibers was assessed by following ASTM F 1635-04 method [88]. Initially, the nanofiber samples were weighed and placed in a 0.1 M PBS solution containing lysozyme (60.100 units/ml) and kept in the incubator at 37℃. After certain intervals of time (1, 30, 60, 90, 120, 150 and 180 days), the samples were

extracted and washed with distilled water, followed by drying in a vacuum oven for 24 hours to remove extra water. Finally, the remaining weight was calculated using a formula, which involved the comparison of the weight before and after the degradation process at a specific interval [103].

$$Weight\ remaining\,(\%) = 100 - \left(\frac{W_0 - W_d}{W_0} \times 100 \right)$$

W_0 and W_d are the weights of the electrospun core-shell PCL/PCL and sample 2's nanofibers before and after degradation for a specific time interval, respectively.

3.5. Cell Culture Studies

Cell culture experiments were conducted using the L929 ATCC CCL-1 mouse fibroblast cell line obtained from the Bioengineering Laboratory at Kirikkale University to assess cell-material interactions. The cells were seeded onto the prepared scaffolds at a concentration of $1x10^5$ cells/ml and cultured in DMEM including 10% FBS and grown at 37°C in a humidified atmosphere with 5% CO2 [106].

Circular samples with a diameter of 1cm were placed in parafilm-coated TCPS (tissue culture polystyrene) wells. Before the culture, the samples were sterilized using UV for 30 min. Cell growth was evaluated using the MTT assay, and the seeded nanofibers were examined using fluorescence and scanning electron microscopes to assess adhesion, growth, and proliferation characteristics.

3.5.1. Cell Attachment Assay

The hemocytometric counting method was used to conduct the Cell Attachment assay at 30-minute intervals for 180 minutes, including 30 m, 60 m, 120 m, 150 m, and 180 m. The unattached cells were removed from each well by discarding the medium after each interval. The sample materials were then incubated with Trypsin/EDTA solution (0.25% wt/vol) for 5 minutes in a 37°C and 5% CO2 incubator, and the attached cells were detached. The remaining cells were counted using trypan blue dye, which stained viable cells blue, for each of the 30-minute intervals. The results were reported as the ratio of viable cells to initially seeded cells [103].

3.5.2. MTT Assay

The MTT (3-[4,5-Dimethylthiazol-2-yl]-2,5-Diphenyltetrazolium Bromide) viability method is a standard test that quantitatively determines the proportion of viable cells in a cell population. According to this method, the dehydrogenase enzyme in the mitochondria of healthy cells cleaves the tetrazolium ring in the MTT dye and forms formazan crystals (Kısmalı, G. and Sel, T. 2012; Mosmann, T. 1983) [107-108]

Core-shell PCL/PCL, core-shell coated with DBD plasma using DAP for 1, 3, and 5 minutes, and electrospun PCL nanofibers were tested. These samples were placed in 96-well plates lined with parafilm and subjected to an MTT cell proliferation assay every 48 hours over a 7-day cell culture period. At the end of each period, 10 µl of MTT solutions (5 mg/mL) were added to each well and incubated at 37°C for three hours in the dark. Then, the medium containing MTT was discarded, 125 µl of DMSO was added to each well, and the formazancrystals precipitated in the wells were dissolved by incubating in the dark for 15 minutes on a shaking table (GFL-3012). The color intensity formed by the formazan crystals was evaluated by measuring absorbances at 570 nm on a microplate reader (LedEtect 96). Color intensity and viable cell ratio show a positive correlation. The ratio of viable cells to concentrations of synthesis compounds is expressed as relative cell viability versus that of controls [108].

The cell viability was compared between the three types of electrospun nanofibers and the control group, which were TCPS Petri dishes. The MTT assay measures the cell proliferation rate as well as the reduction in cell viability due to apoptosis or necrosis, with the viability of the cells being directly related to the level of reduction, which can be easily determined with a spectrometer. Each measurement was repeated three times [105].

3.5.3. Fluorescence Imaging

To study the attachment and proliferation of cells on/within the electrospun sample 1 and sample 2 core-shell structures with DBD plasma-treated DAP-coated PCL/PCL nanofibers and electrospun PCL nanofibers, the samples were stained with Acridine Orange (AO) at a concentration of 25 µg/ml (AO; 25 µl/ml in ethanol) and Propidium Iodide (PI) concentrations of 25 µg/ml (PI; 25 µl/ml in ethanol) solutions. Fluorescent

images were taken on the 3rd, and 7th days of the experiment. To obtain these images, the samples were taken out of the incubator, the medium was discarded, and the nanofibers were washed with PBS three times. The samples were then fixed with 2.5% glutaraldehyde for 30 minutes, stained with AO/PI 1:1 (v./v.) for 10 minutes in the dark, and imaged immediately using a Fluorescent Microscope (AMG EVOS-FL, USA) [103].

3.5.4. Observation with SEM

The morphological features of the cells grown on the modified samples were examined at the end of the 3rd and 7th days of the culture using Scanning Electron Microscopy (SEM). The procedure involved discarding the medium, washing the samples with PBS three times, and fixing the samples with 2.5% glutaraldehyde for 30 min. The samples were then dehydrated with increasing concentrations of ethanol, starting from 30% and ending at 100%, for 2 minutes each. After that, the samples were immersed in 100% hexamethyldisilazane for 5 minutes, air-dried, and coated with a thin layer of Au-Pt (~3 nm) before being imaged with SEM [103].

CHAPTER 4

Results and Discussion

4.1. Production of Electrospun Core-Shell PCL/PCL Scaffolds

To fabricate electrospun untreated core-shell PCL/PCL and sample 1 (DBD plasma with DAP coated at 1, 3, and 5 min) and sample 2 (DBD plasma with DAP coated at 1, 3, and 5 min) nanofibers, solution and process parameters were either gleaned from existing literature or optimized (**Figure 4.1**). The parameters that were determined or optimized, as delineated in Sections 3.2.2 and 3.2.3, were subsequently employed sequentially to generate a series of nanofibers, which were utilized in ensuing characterization studies.

Based on the TEM and SEM analysis outcomes, a comparative examination of the electrospun untreated core-shell PCL/PCL structure between sample 1 and sample 2 has been conducted. As a consequence of this comparison, while a core-shell formation was discernible in the images procured from sample 1, comprehensive results could not be ascertained. In contrast, according to the TEM images provided by sample 2, a core-shell structure was successfully formed, and detailed analysis results were obtained. **In light of this analytical conclusion, sample 1 was excluded, and cell culture experiments proceeded with sample 2.**

Figure 4.1. Core/shell structure of 2% (w/v) PCL/PCL electrospun fiber production.

4.2.Characterizations of Electrospun Core-Shell PCL/PCL Scaffolds

4.2.1. Thickness, The Average Fiber Diameter and The Average Inter-Fiber Pore Size Values of The Prepared Electrospun Scaffolds

Using a micrometer and ImageJ Launcher software program, the thicknesses, average fiber diameter, and average inter-fiber pore size of the scaffolds were measured from SEM and TEM photographs and summarized in (**Table 4.1**.). The measurements showed that the thickness of the prepared scaffolds was relatively consistent, ranging from (0.020 ± 0.002 mm) - (0.020 ± 0.003 mm) - (0.020 ± 0.002 mm) - (0.020 ± 0.003 mm) - (0.020 ± 0.002 mm) for sample 1 and, (0.022 ± 0.002 mm) - (0.022 ± 0.003 mm) - (0.022 ± 0.002 mm) - (0.022 ± 0.002 mm). The average fiber diameter measurements revealed that the electrospun untreated core-shell PCL/PCL scaffold had the smallest average fiber diameter for sample 1 (0.403 ± 0.002 μm) and, while the sample 2 (5 min.) scaffolds had the largest average fiber diameter (0.569 ± 0.002 μm), with sample 2 (5 min.) scaffolds having an intermediate value for average inter-fiber pore size (1.160 ± 0.602 μm).

Table 4.1. Properties of the electrospun PCL and sample 1 and sample 2 scaffolds.

Sample	**Thickness (mm)**	**Average Fiber Diameter (μm)**	**Average Inter-fiber Pore Size (μm)**
E. S. C-S PCL/PCL (Sample 1**)**	**0.020 ± 0.002**	**0.403 ± 0.002**	**1.252 ± 0.422**
1 min.	0.020 ± 0.003	0.472 ± 0.001	1.366 ± 0.211
3 min.	0.020 ± 0.002	0.473 ± 0.001	1.369 ± 0.129
5 min.	0.020 ± 0.003	0.475 ± 0.002	1.372 ± 0.230
E. S. C-S PCL/PCL (Sample 2**)**	**0.022 ± 0.002**	**0.452 ± 0.001**	**2.039 ± 0.503**
1 min.	0.022 ± 0.003	0.557 ± 0.002	2.152 ± 0.705

3 min.	0.022 ± 0.002	0.556 ± 0.001	2.156 ± 0.711
5 min.	0.022 ± 0.002	0.569 ± 0.002	2.160 ± 0.602

4.2.2. Optimization of DBD Plasma

Ar gas + DAP surface modifications with argon gas flow rates of 60, 80, and 100 sccm (standard cubic centimeter) and plasma application time between 0.5, and 5 min, the CA values measured and compared to the untreated samples showed that the plasma surface modifications after 5 min introduced hydrophilicity to the surfaces of electrospun PCL/PCL nanofibers (**Table 4.2 for sample 1** and**, Table 4.3 for sample 2**).

The sample groups treated for more than 5 min. were severely etched to the surface point where they became extremely hydrophilic and flow damaged; therefore, they were unsuitable for use as dental tissue scaffolds. However, inconsistent CA values obtained between 1 and 5 min and naked-eye observations showed that there were several areas on the surfaces of the modified samples that were highly hydrophilic. Thus, the surface modification is thought to cause partial wear of the upper PCL layer. Using the DBD Plasma technique, it was concluded that the electrospun coating with DAP affected the surfaces of PCL/PCL nanofibers. Therefore, the effect of surface modifications of less than 1 min was investigated, and the results showed that the plasma surface modifications caused no significant change in hydrophilicity, but an increase in hydrophobicity (the CA value of 0,5 to 7 min plasma modification is given in Table 4.2 and 4.3 as an example). According to the data, the highest hydrophilicity that could be obtained without physical or chemical damage in this system was found for the modifications carried out under 80 and 100 sccm argon flow rates for 1 min. The CA values of the mentioned samples were slightly above 80°, which was approximately 10° less than that of the untreated electrospun core-shell structured PCL/PCL samples.

This increase in hydrophilicity could be due to the topography as well as introduction to the fiber surfaces during plasma treatment [88]. The surface hydrophilicity of a core-shell electrospun PCL polymer can be easily assessed by measuring the contact angle on the substrate. The contact angles of the untreated and treated PCL/PCL scaffolds

were measured using the sessile drop technique with ultrapure water as the probe liquid. In the sample 1 groups (**Table 4.2.** and sample 2 groups **Table 4.3.)**, the variation of contact angle data on the electrospun core-shell PCL surface with DBD plasma treatment time is given. According to the CA analyses, stable conditions were observed in the values from the sixth day. In particular, for the two sample groups on the seventh and eighth days following the sixth day, CA analyses showed that the DBD plasma method increases the surface hydrophilicity at an observable level on surfaces [90].

Table 4.2. The Contact Angle (°) of electrospun sample 1 group's, untreated core-shell PCL/PCL nanofibers treated with Ar + DAP DBD plasma surface modification.

Flow Rate (sccm)	**Time (min)**						
	0.5 CA (°)	**1 CA (°)**	**2 CA (°)**	**3 CA (°)**	**4 CA (°)**	**5 CA (°)**	**7 CA (°)**
60	**104.307 ±2.1**	93.666 ±2.4	94.693 ±2.1	90.274 ±2.1	80.060 ±1.6	88.221 ±1.6	_
80	**101.710 ±1.6**	90.621 ±2.3	84.195 ±1.1	91.606 ±2.4	80.402 ±1.1	74.007 ±2.1	70.517 ±0.7
100	**102.428 ±2.4**	98.965 ±2.4	81.403 ±2.2	79.271 ±1.1	65.086 ±2.9	52.603 ±1.2	50.420 ±0.5

Table 4.3. The CA(°) values of electrospun sample 2 group's, untreated core-shell PCL/PCL nanofibers treated with Ar + DAP DBD plasma surface modification.

Flow Rate (sccm)	**Time (min)**						
	0.5 CA (°)	**1 CA (°)**	**2 CA (°)**	**3 CA (°)**	**4 CA (°)**	**5 CA (°)**	**7 CA (°)**
60	**100.129 ±1.7**	92.715 ±1.3	93.571 ±1.2	89.072 ±0.6	78.081 ±0.3	83.129 ±0.7	_
80	**98.113 ±0.9**	88.157 ±1.6	85.033 ±1.6	90.109 ±1.1	78.222 ±1.0	71.213 ±1.7	69.349 ±0.4
100	**101.503 ±1.7**	94.667 ±1.8	82.226 ±1.7	81.020 ±0.3	68.901 ±1.3	56.963±0.6	_

4.2.3. Contact Angle Measurements

The effectiveness of DBD plasma surface modifications was evaluated according to untreated electrospun core-shell PCL/PCL nanofiber scaffolds as well as electrospun PCL/PCL fibers coated with DAP monomers. Thus, the CA values of untreated electrospun core-shell PCL/PCL, sample 1 groups, and sample 2 group scaffolds treated with DAP monomer coating on their surfaces using the DBD Plasma technique

were measured and used as a reference (**Table 4.4** and, **Table 4.5**.). As can be seen in (**Table 4.4.** and **Table 4.5.)**, electrospun untreated core-shell PCL/PCL is a hydrophobic material with a CA value above ~90°. On the contrary, the electrospun core–shell is extreme hydrophilic with PCL/PCL surfaces coated with DAP monomer owing to DBD plasma. Electrospun core-shell PCL/PCL nanofibers, the surfaces of which are coated with DAP monomer, have moderate hydrophilicity due to the complex fiber topography resulting from the combination of the same polymers and surface coatings. On the other hand, the goal of plasma surface modifications is to achieve a surface wettability as close as possible to commercial TCPS with a CA value of 49,7° [91]. Therefore, the parameters for DBD plasma surface modifications are based on both the untreated electrospun untreated core-shell PCL/PCL samples and the sample 1 and sample 2 groups coated with DAP monomer, as well as the 1, 3 and 5 min DBD surfaces CA optimized according to their measurements. CA, the wettability analysis results were taken between 1 and 8 days with a 24-hour decrease every day. The results were obtained between 1. and 8. days (**Table 4.4.** and **Table 4.5.)** as prepared. According to the results of this analysis, if it is necessary to make assumptions, the results between six and eight days give decently close results to each other. The CA results varied according to the material surface structures and production minutes from the first day to the last day. Considering this diversity and distribution, and the application of the DBD plasma, the surfaces showed more hydrophilic properties compared to the electrospun untreated core-shell PCL/PCL specimens. In 8-day study, the most stable surface property was demonstrated by a sample that was electrospun and subjected to DBD plasma surface treatment for 5 min at 100 sccm.

Table 4.4. The CA (°) of sample 1; 1 min, 3 min, and 5 min DBD Plasma (Argon gas (DAP carrier)) used surfaces coated with DAP monomer electrospun core-shell PCL/PCL nanofibers.

Contact Angle Values (with 100 sccm)	
Sample 1	**Contact Angle (C.A.) (°)**
1st Day	
Electrospun Core-Shell PCL/PCL	106.52 ± 0.58
DBD Plasma (1 min)	91.07 ± 0.76
DBD Plasma (3 min)	62.19 ± 0.23
DBD Plasma (5 min)	54.22 ± 0.31
2nd Day	
Electrospun Core-Shell PCL/PCL	106.30 ± 1.63
DBD Plasma (1 min)	88.15 ± 0.45
DBD Plasma (3 min)	60.48 ± 0.35
DBD Plasma (5 min)	53.70 ± 0.23
3rd Day	
Electrospun Core-Shell PCL/PCL	104.30 ± 1.06
DBD Plasma (1 min)	87.91 ± 0.33
DBD Plasma (3 min)	60.36 ± 0.57
DBD Plasma (5 min)	52.06 ± 0.29
4th Day	
Electrospun Core-Shell PCL/PCL	104.04 ± 0.87
DBD Plasma (1 min)	88.29 ± 0. 69
DBD Plasma (3 min)	60.44 ± 0.77
DBD Plasma (5 min)	47.66 ± 0.82
5th Day	
Electrospun Core-Shell PCL/PCL	103.04 ± 0.92
DBD Plasma (1 min)	87.89 ± 0.63
DBD Plasma (3 min)	60.40 ± 0.13
DBD Plasma (5 min)	47.59 ± 0.28

6th Day	
Electrospun Core-Shell PCL/PCL	102.52 ± 0.31
DBD Plasma (1 min)	85.73 ± 0.43
DBD Plasma (3 min)	61.29 ± 0.58
DBD Plasma (5 min)	44.11 ± 0.55
7th Day	
Electrospun Core-Shell PCL/PCL	103.07 ± 0.14
DBD Plasma (1 min)	85.42 ± 0.66
DBD Plasma (3 min)	60.74 ± 0.36
DBD Plasma (5 min)	44.09 ± 0.29
8th Day	
Electrospun Core-Shell PCL/PCL	102.38 ± 0.56
DBD Plasma (1 min)	85.00 ± 0.34
DBD Plasma (3 min)	60.16 ± 0.65
DBD Plasma (5 min)	44.02 ± 0.26

Table 4.5. The contact angle (°) of sample 2; 1 min, 3 min, and 5 min DBD Plasma (Argon gas (DAP carrier)) used surfaces coated with DAP monomer electrospun core-shell PCL/PCL nanofibers.

Contact Angle Values (with 100 sccm)	
Sample 2	**Contact Angle (C.A.) (°)**
1st Day	
Electrospun Core-Shell PCL/PCL	107.66 ± 0.43
DBD Plasma (1 min)	97.33 ± 0.12
DBD Plasma (3 min)	71.32 ± 0.22
DBD Plasma (5 min)	59.29 ± 0.40
2nd Day	
Electrospun Core-Shell PCL/PCL	107.39 ± 0.35
DBD Plasma (1 min)	95.53 ± 0.49
DBD Plasma (3 min)	69.87 ± 0.37
DBD Plasma (5 min)	57.63 ± 0.81

3rd Day	
Electrospun Core-Shell PCL/PCL	97.74 ± 0.73
DBD Plasma (1 min)	93.23 ± 0.47
DBD Plasma (3 min)	68.55 ± 0.32
DBD Plasma (5 min)	57.06 ± 0.75
4th Day	
Electrospun Core-Shell PCL/PCL	87.51 ± 0.21
DBD Plasma (1 min)	79.00 ± 0.76
DBD Plasma (3 min)	67.51 ± 0.80
DBD Plasma (5 min)	50.54 ± 0.89
5th Day	
Electrospun Core-Shell PCL/PCL	72.31 ± 0.11
DBD Plasma (1 min)	65.69 ± 0.72
DBD Plasma (3 min)	55.72 ± 0.20
DBD Plasma (5 min)	47.03 ± 0.38
6th Day	
Electrospun Core-Shell PCL/PCL	71.09 ± 0.50
DBD Plasma (1 min)	65.51 ± 0.73
DBD Plasma (3 min)	47.74 ± 0.12
DBD Plasma (5 min)	44.77 ± 0.22
7th Day	
Electrospun Core-Shell PCL/PCL	71.03 ± 0.22
DBD Plasma (1 min)	64.65 ± 0.29
DBD Plasma (3 min)	47.92 ± 0.31
DBD Plasma (5 min)	43.36 ± 0.13
8th Day	
Electrospun Core-Shell PCL/PCL	70.66 ± 0.34
DBD Plasma (1 min)	63.82 ± 0.45
DBD Plasma (3 min)	44.34 ± 0.10

DBD Plasma (5 min)	42.12± 0.21

4.2.4. Scanning Electron Microscope (SEM) Analysis

The morphologies of the nanofibers were observed by scanning electron microscopy (SEM). SEM micrographs and diameter distributions of the electrospun PCL/PCL core-shell scaffolds with different weight ratios are shown in (**Figure 4.2** and, **Figure 4.3**.). It is easy to form continuous nanofibers, which may show a large number of homogeneous structures [92-93]. The surfaces of the electrospun PCL/PCL nanofibers were modified using the DBD plasma method and coated with DAP (**Figure 4.2**). It can be seen that the core-shell scaffolds have a smooth and homogeneous morphology. The topography of the PCL surfaces can change after DBD plasma treatment.

In the case of the PCL samples, SEM images revealed the surface features and changes that occurred after the DBD plasma treatment. The images show increase in the surface roughness, with the appearance of cracks, pores, and other surface features that were not present before the treatment. The surface may also appear more textured or etched owing to the effect of the plasma on the surface. The exact appearance of the SEM images of PCL samples after DBD plasma treatment depends on various factors, such as the treatment time, power, and gas used for the plasma treatment, as well as the initial morphology and composition of the PCL sample [103].

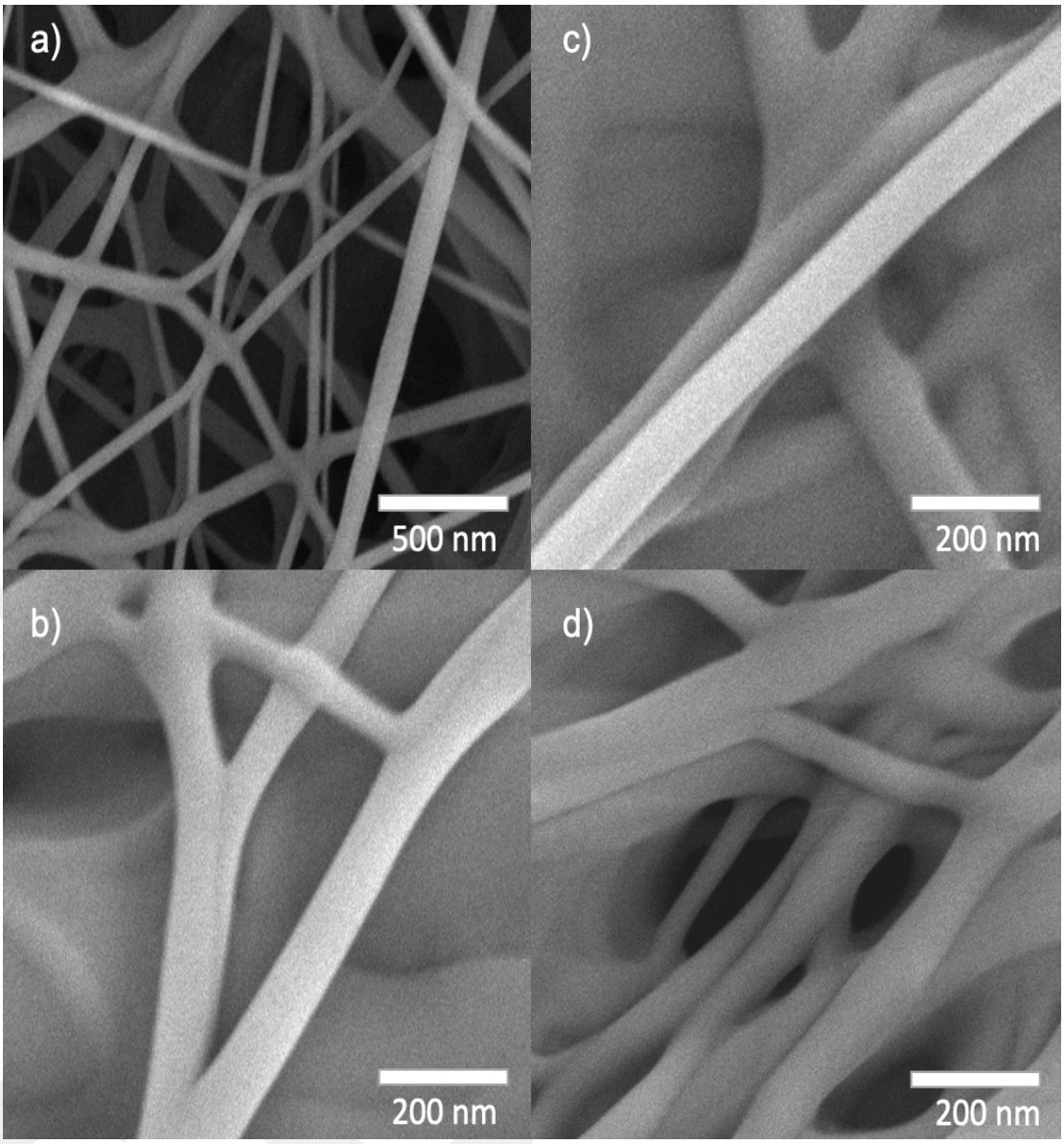

Figure 4.2. SEM images of coaxiall electrospun a) PCL/PCL fibers, b) PCL/PCL, 1 min. DBD Plasma with DAP coated surfaces x20000 and c) PCL/PCL, 3 min. DBD Plasma with DAP coated surfaces x20000, d) PCL/PCL, 5 min. DBD Plasma with DAP coated surfaces x20000.

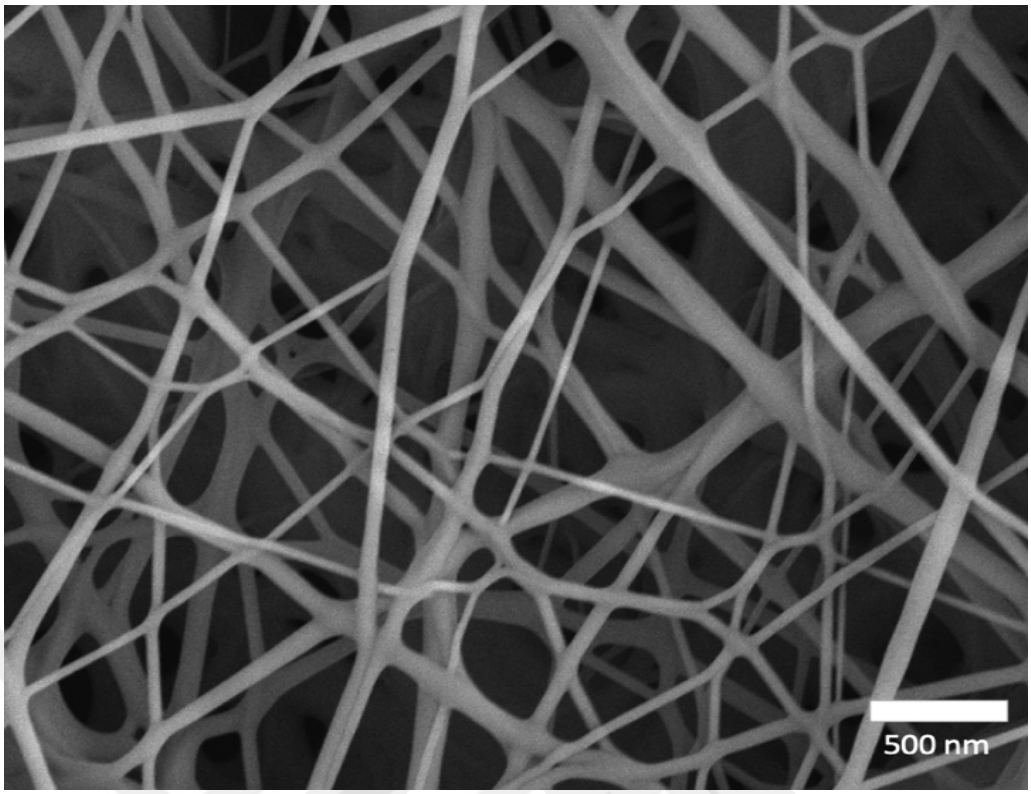

Figure 4.3. SEM image of electrospun core-shell PCL/PCL nanofibers.

Research has shown that argon gas DBD plasma treatment can influence the topography of electrospun PCL fibers in a controllable manner. In particular, plasma treatment can create surface features such as pits and grooves, which can affect the behavior of cells and tissues [95-96].

The effect of argon gas plasma treatment on the topography of the electrospun PCL fibers can be attributed to several factors. First, plasma can etch away surface protrusions or roughness, resulting in a smoother fiber surface. Second, plasma can create surface features by selectively etching certain regions of the fiber surface. The creation of surface features depends on the plasma parameters used, such as the gas flow rate, treatment time, and power [97-98].

Studies have investigated the effect of argon plasma treatment on the topography and cell behavior of electrospun PCL fibers. For example, Kuo et al. (2015) found that plasma treatment with argon gas could increase the fiber diameter and create surface features such as pits and grooves [99]. The surface features created by plasma treatment resulted in increased cell adhesion and proliferation.

Similarly, Wu et al. (2018) found that argon plasma treatment increased the fiber diameter and created surface features that enhanced cell adhesion and proliferation [100].

The mechanism underlying the enhanced cell behavior on electrospun PCL fibers with surface features created by argon plasma treatment is still under investigation. However, it has been proposed that surface features can influence the conformation of adsorbed proteins, which in turn can affect the cellular behavior. For example, proteins may preferentially adsorb onto the surface features, leading to changes in cell adhesion and proliferation.

In conclusion, argon gas DBD plasma treatment is a controllable technique for modifying the topography of electrospun PCL fibers. Plasma treatment can create surface features that influence the behavior of cells and tissues. The mechanism behind the enhanced cell behavior on electrospun PCL fibers with surface features is still under investigation, but is believed to be related to changes in protein adsorption [104].

4.2.5. Transmission Electron Microscope (TEM) Analysis

TEM observations (FEI Tecnai G2 Spirit BioTwin CTEM, (USA)) were carried out to determine the PCL/PCL core-shell structure of the coaxial electrospun fibers. The samples for TEM observation were prepared by placing a carbon-coated copper grid on the collector to directly deposit a very thin layer of electrospun fibers on the grid. Then, a copper grid containing fiber staining was used to obtain the TEM image by passing a beam of electrons through. The TEM analysis results were scaled using the ImageJ program and sorted alphabetically (**Figure 4.4.** and**, Figure 4.5.**).

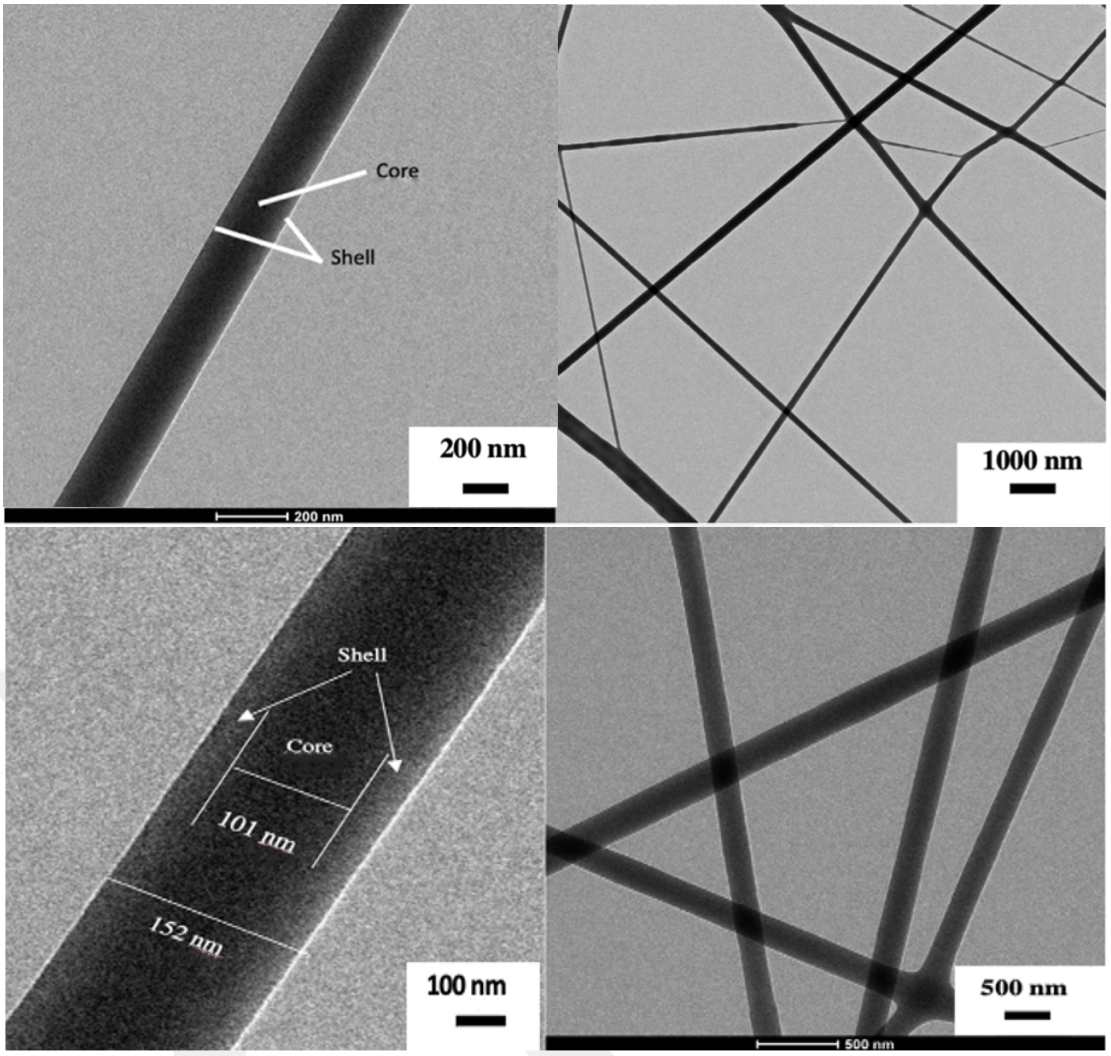

Figure 4.4. TEM images demonstrate the core-shell structure of the coaxially electrospun fibers. DCM solvent was used in the core part and Chloroform solvent was used in the shell region.

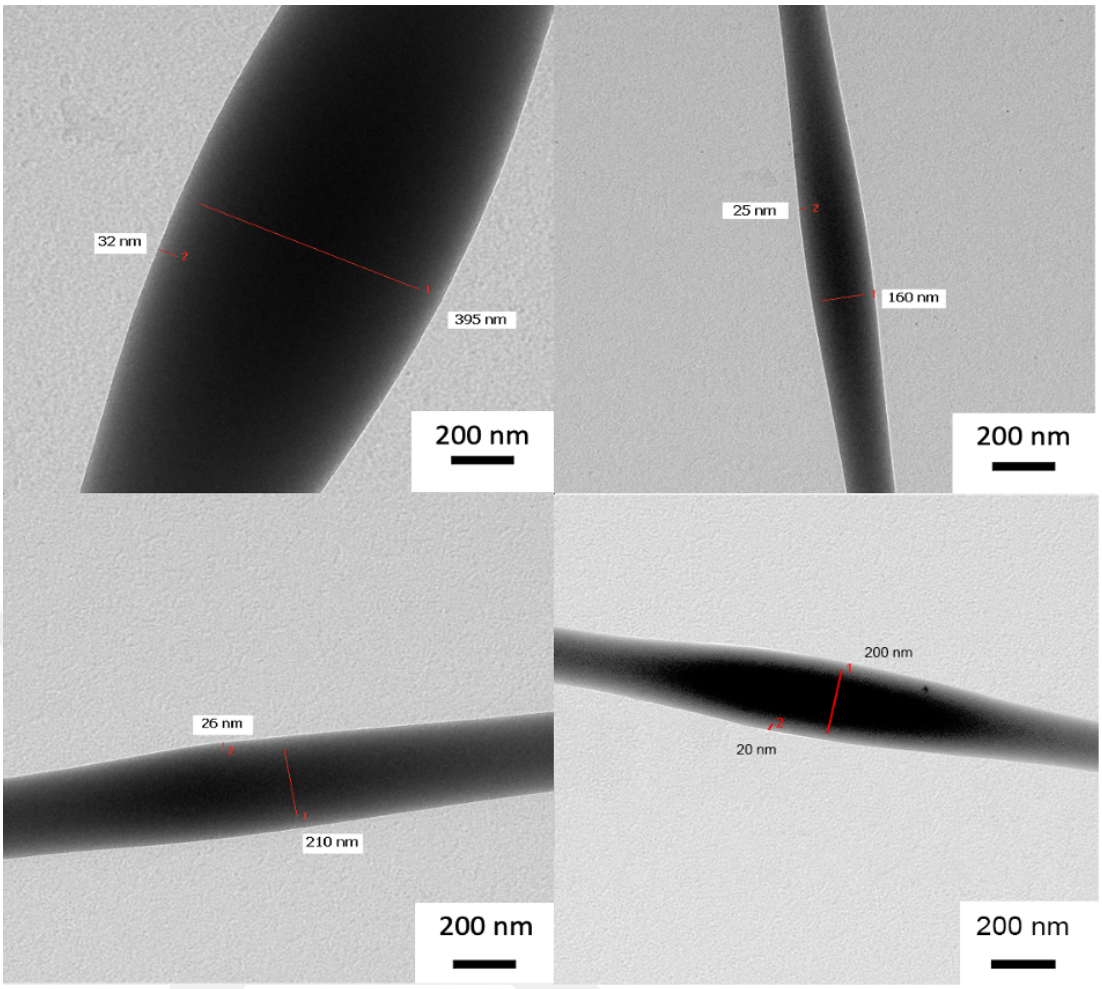

Figure 4.5. TEM images demonstrate the core-shell structure of the coaxially electrospun fibers. Chloroform solvent was used in the core part and DCM solvent was used in the shell region.

The core-shell membranes were prepared using coaxial needles with a core needle inner diameter of 0.57 mm and a shell needle inner diameter of 1.6 mm. The core and shell solution feed rates were 10 µL/min and 15 µL/min, respectively. To study the core-shell structure, we used TEM to observe and demonstrate the core-shell formation. Because electrons penetrate very thin samples (<100 nm), TEM was used to study the internal structure of the fibers, and SEM characterization was used to study the surface structure of the samples.

In the prepared core-shell membranes for sample 1, core PCL was dissolved in DCM/methanol and shell PCL was dissolved in a chloroform/methanol mixture.

On the other hand, for sample 2, core PCL was dissolved in chloroform/methanol, and shell PCL was dissolved in a DCM/methanol mixture.

Additionally, in Sample 1, the core of the PCL structure was fully surrounded by the PCL shell structure; however, the shell was much finer than the nanoscale core, which was quite thick. This is due to the fact that the feeding rate of the core was significantly greater than that of the shell, which aligns with previous research findings. [101].

From the results of the second experiment, the core-shell PCL/PCL structure was obtained, and the viscous properties in the core-shell were analyzed. Because chloroform and DCM solutions are good solvent solutions for PCL, they were used in the second experimental group, such as sample 2 groups in the core to prove that the chloroform solvent shows less viscous properties, and in the shell region to prove that the viscosity of the DCM solvent is high. According to the literature, no core-shell structure could be obtained in obtaining the PCL/PCL structure, whereas the core-shell structure could not be obtained in TEM imaging of the electrospun PCL/PCL structure produced [88]. In this context, when the viscosity properties of the electrospun PCL/PCL structure were examined, a chloroform solution with low viscosity was taken to the core side and the DCM solution with high viscosity was taken to the shell side, and the core-shell structure was successfully obtained with TEM imaging (**Figure 4.5.**).

4.2.6. Mechanical Properties

The strength of nanofiber scaffolds is a critical factor for their use in dental soft tissue engineering. At (**Figure 4.6.)** and (**Table 4.6.)** provides an overview of the mechanical properties of various dental scaffolds, including their Elastic Modulus and Tensile Strength. The average Elastic Modulus and Tensile Strength values of the untreated core-shell PCL/PCL nanofibers and 1min., 3 min. and 5 min. nanofibers were found to be 4.940 ± 0.002, 3.825 ± 0.002, 2.952 ± 0.001, 2.171 ± 0.001 and 3.265 ± 0.001, 7.652 ± 0.002, 5.020 ± 0.001, 2.156 ± 0.002 respectively.

It was observed that the untreated core-shell PCL/PCL scaffolds mechanical properties compared to the core-shell PCL/PCL scaffolds coated with DBD plasma technique for 1, 3, and 5 minutes using DAP on their surfaces. However, the electrospun untreated

core-shell PCL/PCL scaffolds showed increased Elastic Modulus (4.940 ± 0.002) and, but lower Tensile Strength (3.265 MPa ± 0.001), and decreased the strain at break value (0.66% ± 0.772), especially in comparison to the electrospun core-shell PCL/PCL scaffolds coated with DBD plasma technique for 1, 3 and 5 min. using DAP on their surfaces. This the electrospun core-shell PCL/PCL scaffolds coated with DBD plasma technique for 3 and 5 min. using DAP on their surfaces increase in mechanical properties can be attributed to the smoother surface of the scaffolds caused by the DBD plasma surface etching effect, resulting in reduced nanofiber diameters and shorter fracture points.

Furthermore, the structure of the electrospun untreated core-shell PCL/PCL and 5-min. DBD plasma-coated DAP surfaces showed decreased elastic and plastic deformation under the same amount of applied load. Additionally, it was observed that the electrospun untreated PCL/PCL core-shell scaffold structures exhibited more brittle properties. On the other hand, the DBD plasma-coated samples subjected to DAP monomer and plasma treatment for 3 and 5 minutes showed an even more fragile state due to the abrasion of fiber sizes caused by DBD plasma and the achievement of a smoother surface through DBD plasma. As a result, this led to a decrease in elongation at the point of failure.

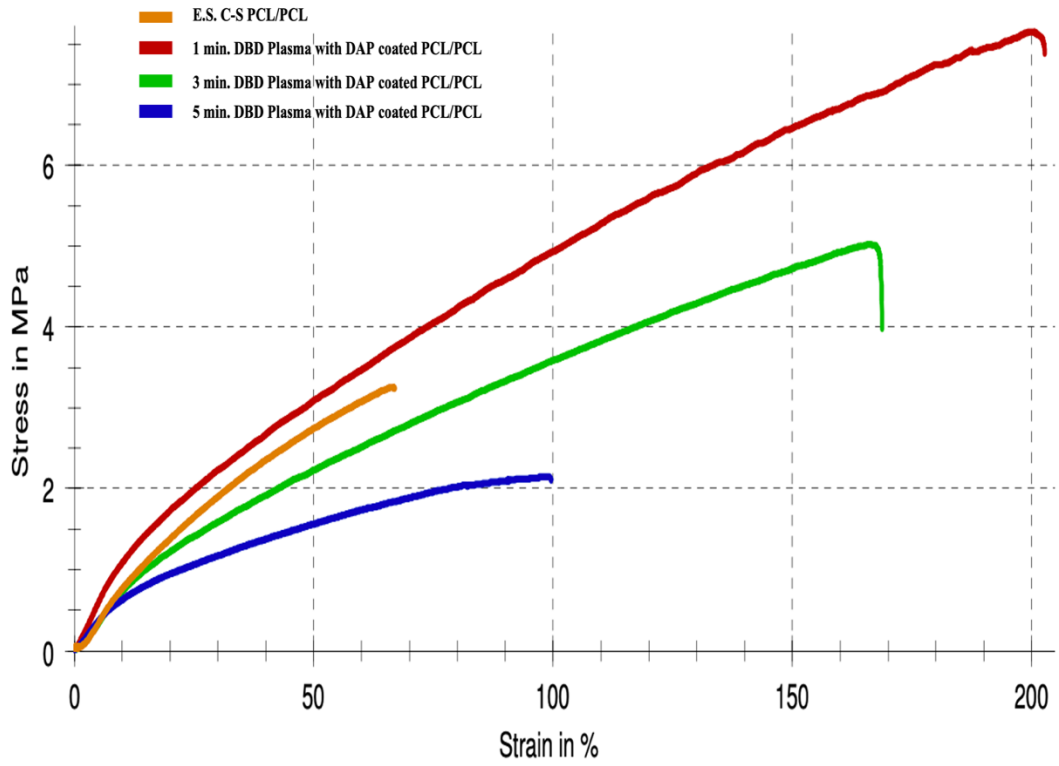

Figure 4.6. Tensile properties of the scaffolds.

Table 4.6. Mechanical testing results of scaffolds.

Sample	Elastic Modulus (MPa)	Tensile Strenght (MPa)	Strain at break (%)
E.S. C-S PCL/PCL	4.940 ± 0.002	3.265 ± 0.001	0.66 ± 0.77
1 min. DBD Plasma with DAP coated PCL/PCL	3.825 ± 0.002	7.652 ± 0.002	2 ± 0.63
3 min. DBD Plasma with DAP coated PCL/PCL	2.952 ± 0.001	5.020 ± 0.001	1.7 ± 0.26
5 min. DBD Plasma with DAP coated PCL/PCL	2.171 ± 0.001	2.156 ± 0.002	0.99 ±0.56

4.2.7. Fourier Transform Infrared Spectroscopy (FTIR) Analysis

The organic groups of electrospun untreated core-shell PCL/PCL and the electrospun core-shell PCL/PCL surfaces were treated with DAP coating using the DBD plasma technique for 1 minute, 3 minutes, and 5 minutes nanofibers with different time periods were analyzed by FTIR and shown in the (**Figure 4.7**.) FTIR spectra revealed the characteristic bands for a) electrospun untreated core-shell PCL/PCL at 2860 to 2865 cm^{-1} symmetric ν_{CH2} strecthing, for asymmetric ν_{CH2} band at 2930 to 2970 cm^{-1} and ν_{C-H} band at 2860 cm^{-1}, for $\nu_{C=O}$ carbonyl group band at 1725 to 1730 cm^{-1}, for ν_{CH2} bending (scissoring and rocking) band can be seen at 1410 to 1470 cm^{-1}, for ν_{C-O-C} ester linkage 1260 cm^{-1}, for ν_{O-C-C} stretching band seen on at 1090 to 1120 cm^{-1} and for ν_{C-C} strecthing in the crystalline region can be seen at 800 to 850 cm^{-1}.

The FTIR spectrum clearly showed that the characteristic bands of the electrospun core-shell PCL/PCL sample surfaces treated for 1 minute were similar in peak intensity to those coated with DAP monomer using the DBD plasma technique, as shown in the graph. When comparing the FTIR spectrum, b) and c) graphs, it is evident that the coating of the surfaces with DAP monomer using DBD plasma, as shown in b) graph, resulted in a time-dependent change, and the $\nu_{P=O}$ peaks in the c) graph were accelerated by the phosphate group of DAP monomer, becoming elevated in the range of 1100-1200 cm^{-1}.

When comparing the FTIR results for c) and d) spectra, an increase in the peak intensity of the $\nu_{P=O}$ band was observed due to the strengthening of the phosphate bonds of the DAP monomer over time. Furthermore, the stretching intensities of the ν_{P-O-C} band were found to increase with the waiting time of the phosphate groups. The DAP monomer also affected the peaks of the phosphate and alkyl groups, and after the coating process using the DBD plasma technique, it was found that the $\nu_{P=O}$ band varied between 1250 and 1260 cm^{-1} and the ν_{P-O-C} band varied between 900 and 1100 cm^{-1} in intensity, indicating an increase in the phosphate and alkyl groups.

The FTIR analysis results for each separate sample have been obtained and specific characterization ranges have been examined individually and provided as (**Figure 4.7**.)

Generally, in the FTIR analysis, there are similarities between electrospun untreated core-shell PCL/PCL samples and those with surfaces coated with DAP using the DBD plasma technique. Due to the DAP monomer, the formation of phosphate groups affected the $\nu_{P=O}$ and ν_{P-O-C} peaks by intensifying them and influencing the alkyl group, resulting in the enhancement of the $\nu_{C=C}$ peak intensities.

These formed groups and the effect of the DAP monomer on the spectrometry via DBD plasma led to a change in peak intensities. Comparing these changes with the CA (°) values of the samples indicated that they were made more hydrophilic. This was understood to play a significant role in improving biocompatibility, higher cell attachment on the surface and drug delivery studies, as observed.

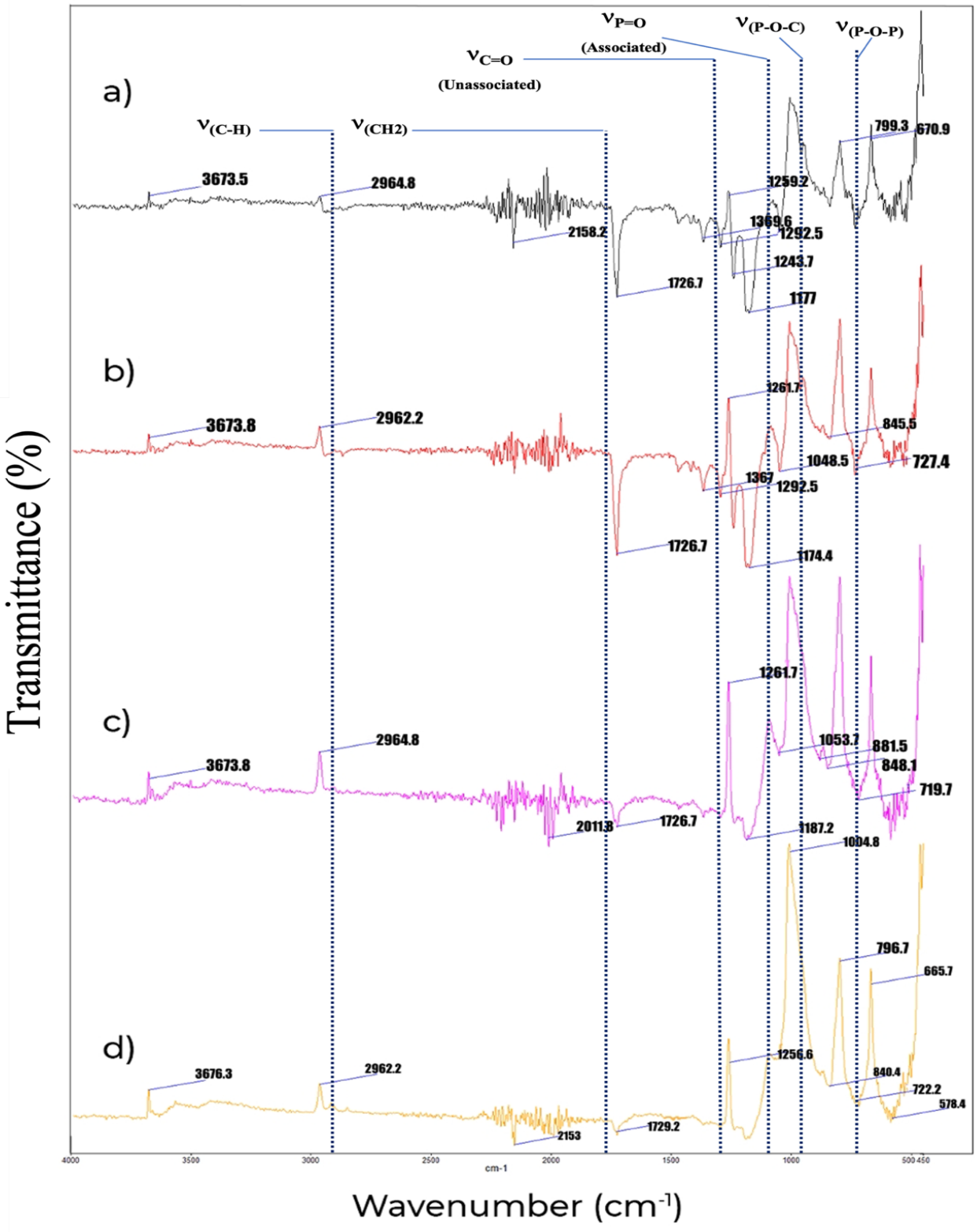

Figure 4.7. FTIR analyzes of the a) electrospun PCL/PCL, b) 1 minutes DBD Plasma with DAP coated electrospun PCL/PCL, c) 3 minutes DBD Plasma with DAP coated electrospun PCL/PCL and, d) 5 minutes DBD Plasma with DAP coated electrospun PCL/PCL samples.

4.2.8. PBS Absorption and Shrinkage Tests

The PBS absorption and shrinkage characteristics of the prepared samples are listed in (**Table 4.7 and 4.8**.) According to the tables, it was seen that the lowest PBS absorption (%) value was measured for core-shell untreated electrospun PCL/PCL (control group) nanofibers (~70% and, ~71% respectively.) because of its relatively more hydrophobic structure compared to those of the other samples. On the other hand, owing to its more hydrophilic characteristics, the highest PBS absorption (%) value was measured for sample 1 and sample 2 groups with 5 min DBD plasma in DAP-coated surface nanofibers (~81% and ~83%, respectively), followed by sample 1 and sample 2 groups with 3 min DBD plasma in DAP-coated surface nanofibers (~79% and, ~80% respectively) and sample1 and sample 2 groups with 1 min DBD plasma in DAP-coated surface nanofibers (~75% and ~77%, respectively). This phenomenon was also observed for shrinkage (%) values because the greater absorption of PBS caused more shrinkage due to the area change of the samples [88]. When comparing sample 2 with sample 1, it has been observed that the PBS absorption and shrinkage percentages of the sample 2 group vary depending on the internal structure and plasmas of the samples. The higher measurements of pore size and fiber diameters have been calculated for sample 2, which is the reason for the increased PBS and shrinkage percentages. The results obtained in this study were consistent with the results obtained from the CA measurements.

Table 4.7. PBS absorption (%) and shrinkage (%) values of the sample 1.

Sample 1	**PBS Absorption (%)**	**Shrinkage (%)**
Electrospun PCL/PCL	70.07 ± 0.6	2.1 ± 0.5
DBD modificated Electrospun PCL/PCL (1 min.)	75.12 ± 0.8	2.2 ± 0.6
DBD modificated Electrospun PCL/PCL (3 min.)	79.06 ± 0.2	4.7 ± 0.7
DBD modificated Electrospun PCL/PCL (5 min.)	81.26 ± 0.5	5.5 ± 0.9

Table 4.8. PBS absorption (%) and shrinkage (%) values of the sample 2.

Sample 2	**PBS Absorption (%)**	**Shrinkage (%)**
Electrospun PCL/PCL	71.11 ± 0.7	4.7 ± 0.4
DBD modificated Electrospun PCL/PCL (1 min.)	77.20 ± 0.4	3.2 ± 0.2
DBD modificated Electrospun PCL/PCL (3 min.)	80.01 ± 0.6	3.1 ± 0.1
DBD modificated Electrospun PCL/PCL (5 min.)	83.23 ± 0.2	5.1 ± 0.4

4.2.9. Water Vapor Transmission Rate (WVTR)

One of the most challenging problems in tooth extraction and periodontal wound treatment is bleeding at the wound site, which can be influenced by the patient's age, health status, blood-thinning medications, and oral health. This situation can lead to an increased risk of infection, swelling, and pain at the wound site. Therefore, a dental wound dressing should quickly prevent or at least reduce bleeding; that is, by controlling absorption and transmission, and accelerating the epithelialization process due to the high moisture in the dental wound area. On the other hand, if the water vapor transmission rate (WVTR) is low, it can inhibit the formation of hemostasis, which may result in a slowdown of the healing process and an increased risk of acute inflammation. The water vapor transmission of a dental wound dressing should prevent excessive dehydration and promote the formation of hemostasis. WVTR results for four types of scaffolds are shown in (**Table 4.9**.) The electrospun untreated core-shell PCL/PCL scaffold has the lowest average WVTR value among the scaffolds. The meaningful WVTR values obtained for this scaffold are due to its lowest average inter-fiber pore size when compared with other scaffolds. The average WVTR values for DBD plasma-treated DAP-coated core-shell electrospun PCL/PCL scaffolds are higher than those of the electrospun untreated core-shell PCL/PCL scaffold. The highest WVTR value belongs to the DBD plasma-treated DAP-coated core-shell electrospun PCL/PCL scaffolds (5 min.). The increased average inter-fiber pore size in the DBD plasma-treated DAP-coated core-shell electrospun PCL/PCL scaffolds significantly supports the results obtained here. The developed DBD plasma-treated DAP-coated core-shell electrospun PCL/PCL scaffolds (5 min.) were observed to meet the requirements of an ideal dental soft tissue wound dressing in terms of water vapor transmission rate. Therefore, it can be concluded that the DBD plasma-treated DAP-coated core-shell electrospun PCL/PCL scaffolds (5 min.) may serve as suitable wound dressings for dental wound site treatment. High water vapor permeability values can accelerate the healing process by maintaining an adequate moisture balance in the wound area and reducing the risk of acute inflammation. In this study, DBD plasma-treated DAP coated core-shell electrospun PCL/PCL scaffolds demonstrate significant potential for developing suitable wound dressing for dental soft tissue treatment.

Table 4.9. Water vapor transmission rate of sample 1's electrospun core-shell PCL/PCL, 1 minutes DBD Plasma with DAP coated electrospun PCL/PCL scaffolds, 3 minutes DBD Plasma with DAP coated electrospun PCL/PCL, 5 minutes DBD Plasma with DAP coated electrospun PCL/PCL, sample 2's electrospun core-shell PCL/PCL, 1 minutes DBD Plasma with DAP coated electrospun PCL/PCL, 3 minutes DBD Plasma with DAP coated electrospun PCL/PCL, 5 minutes DBD Plasma with DAP coated electrospun PCL/PCL.

Samples	**WVTR ($g/m^2.day$)**
Sample 1 (Untreated Electrospun PCL/PCL)	2122 ± 2.1
DBD modificated Electrospun PCL/PCL (1 min.)	2158 ± 2.2
DBD modificated Electrospun PCL/PCL (3 min.)	2160 ± 2.2
DBD modificated Electrospun PCL/PCL (5 min.)	2163 ± 2.1
Sample 2 (Untreated Electrospun PCL/PCL)	2156 ± 1.6
DBD modificated Electrospun PCL/PCL (1 min.)	2163 ± 2.3
DBD modificated Electrospun PCL/PCL (3 min.)	2169 ± 1.4
DBD modificated Electrospun PCL/PCL (5 min.)	2177 ± 2.7

4.2.10. In Vitro Degradation

The degradation of electrospun core-shell untreated PCL/PCL and electrospun core-shell PCL/PCL samples were using DBD plasma and coated with DAP for 1, 3, and 5 minutes scaffolds were studied, and their weight remaining after degradation was recorded in (**Figure 4.8**.). The results showed that electrospun core-shell untreated PCL/PCL scaffolds had a slower degradation rate compared to electrospun core-shell PCL/PCL samples were using DBD plasma and coated with DAP for 1, 3, and 5

minutes scaffolds after 30 days of incubation. Electrospun core-shell untreated PCL/PCL showed minimum weight loss due to having lower hydrophilicity and smaller pore size, while electrospun core-shell PCL/PCL samples were using DBD plasma and coated with DAP for 5 minutes scaffold had the highest degradation rate, resulting in ~10.1% weight loss in just 30 days. As the weight remaining increased, the degradation rate decreased. After 30 days of incubation, the weight loss values were ~15.6% and ~22.2% for electrospun core-shell untreated PCL/PCL and electrospun core-shell PCL/PCL sample was using DBD plasma and coated with DAP for 5 min. scaffolds, respectively. After 60 days, electrospun core-shell PCL/PCL sample was using DBD plasma and coated with DAP for 5 min. scaffold showed the highest weight loss value (30.2%), which could be due to the smooth and larger pore size allowing increased exposure to lysozyme and higher degradation rates.

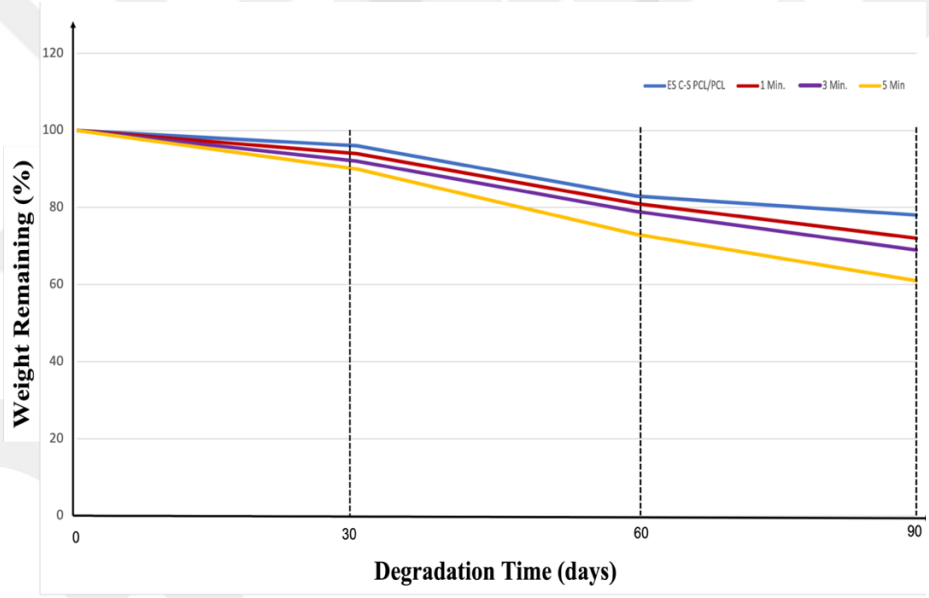

Figure 4.8. Weight remaining of different electrospun core-shell untreated PCL/PCL and electrospun core-shell PCL/PCL samples were using DBD plasma and coated with DAP for 1, 3, and 5 min. scaffolds as a function of degradation time.

4.3. Cell Culture Studies

4.3.1. Cell Attachment Assay

The cell attachment assay is often viewed as the initial stage in cell culture research and is essential for understanding cell-material interactions and various cell behaviors,

such as proliferation, attachment, cell guidance, and differentiation [103]. The percentage of cells attached to the surfaces of the fabricated scaffolds after three hours is depicted in (**Figure 4.9.)**. Tukey's Test was employed to determine the level of significance, with a significance threshold of $p < 0.05$. Data were marked with (*) for $p < 0.05$, (**) for $p < 0.01$, and (***) for $p < 0.001$. According to Tukey's Test, all data were significantly different from each other at $p < 0.001$. As shown in (**Figure 4.9**.), L929 mouse fibroblast cells successfully adhered to the surfaces of all four scaffolds as well as the TCPS, which served as the control group. Despite the presence of electrospun core-shell nanofibers on the surfaces of untreated core-shell PCL/PCL, the material exhibited high hydrophobicity. The literature indicates that increased hydrophobicity can lead to reduced cell attachment on surfaces [103].Therefore, the electrospun core-shell PCL/PCL scaffold with DAP monomer-coated surfaces using 5 min. DBD Plasma, although highly hydrophilic, shows slightly lower hydrophilicity compared to the 3 min. DBD Plasma treated and DAP monomer-coated electrospun core-shell PCL/PCL nanofiber surfaces, as well as the 1 min. DBD Plasma treated and DAP monomer-coated electrospun core-shell PCL/PCL, and the untreated electrospun core-shell PCL/PCL scaffold. In this comparison, the electrospun core-shell PCL/PCL scaffold with less hydrophilic surfaces coated with DAP monomer using 3-minute DBD plasma still allowed a greater degree of cell attachment than the scaffold with more hydrophilic surfaces coated with DAP monomer using 5-minute DBD plasma. The former scaffold exhibited the highest cell attachment rate among all the samples. Moreover, the proportion of attached cells in the TCPS control group is lower than that in all the produced electrospun core-shell scaffolds. Even though electrospun untreated core-shell PCL/PCL exhibit high hydrophobicity, surface porosity plays a crucial role in cell attachment. The highly porous structure of the fabricated electrospun layers promotes cell adhesion to the surface, providing more sites for cells to attach and proliferate [105].

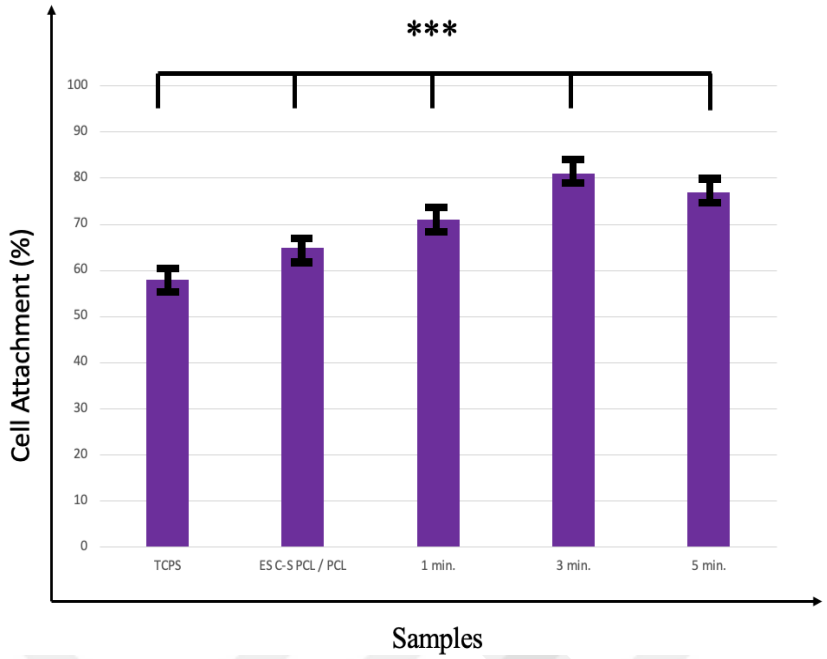

Figure 4.9. The cell attachment percentages of TCPS (control group), E. S. C-S PCL/PCL, 1 min. DBD (DAP) PCL/PCL, 3 min. DBD (DAP) PCL/PCL and, 5 min. DBD (DAP) PCL/PCL samples after 3 h. (***) for $p < 0.001$.

4.3.2. MTT Assay

The cell viability of the fabricated scaffolds was evaluated using the MTT assay over a 7 day period, with measurements taken on days 1st, 3rd, 5th, and 7th. TCPS and electrospun core-shell untreated PCL/PCL specimens served as control groups to investigate the influence of the scaffolds on mouse fibroblast cell proliferation. The results depicted in (**Figure 4.10.)** reveal that cells successfully adhered to all materials and TCPS on the first day, and cell proliferation reached its zenith on day 7th. It was observed that fibroblast cells exhibited a preference for smooth surfaces over rough ones, as evidenced by their higher attachment to the 5 min. DBD (DAP) PCL/PCL surfaces on day 1st. The 1 min. DBD (DAP) PCL/PCL surfaces, which featured electrospun core-shell nanofibers, displayed the lowest absorbance values on day 1st, indicating a diminished preference for the rougher surfaces. This predilection for smooth surfaces by fibroblast cells was evident on days 1st and 3rd. On days 1st, 3rd, 5, and 7th, all absorbance values were significantly distinct from one another, with $p < 0.001$ (***).

On day 5th, a considerable disparity between the control group and the samples was observed, but no significant difference between the sample absorbance values was noted. This could be attributed to enhanced cell proliferation [105]. As cell numbers increased, cells may have proliferated more on the smooth, porous core-shell electrospun regions of the 3 min. and 5 min. DBD (DAP) PCL/PCL samples. As previously stated, a porous and smooth structure offers more sites for cell growth and proliferation, resulting in the highest absorbance values for the 5 min. DBD (DAP) PCL/PCL scaffold and the lowest for the 1 min. DBD (DAP) PCL/PCL scaffold at the conclusion of the cell culture period.

In summary, the MTT assay study demonstrated that the scaffold surfaces, which were subjected to DBD plasma treatment for 1, 3, and 5 minutes and incorporated DAP monomer, exhibited increased cell attachment over time. This can be attributed to both the surfaces becoming smoother in direct proportion to the plasma duration, leading to an increase in porosity, and the DAP monomer exerting a positive effect on the material coating and cell adhesion.

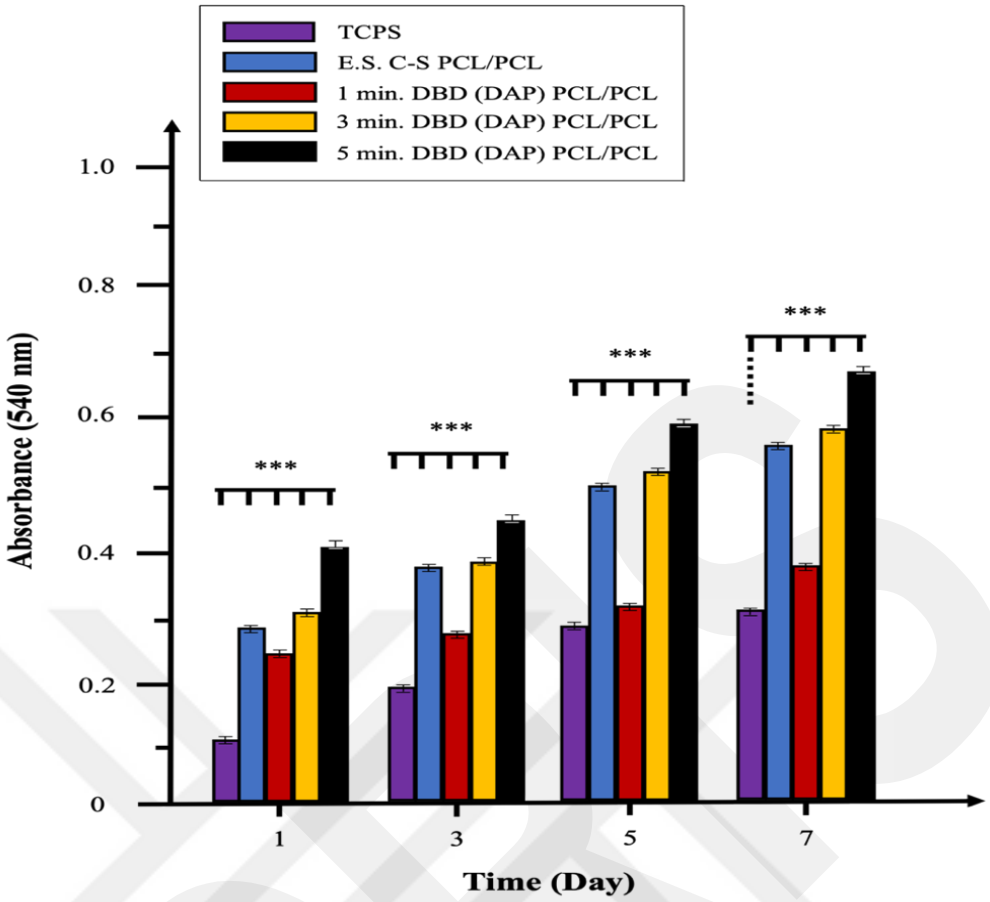

Figure 4.10. The MTT assay absorbance outcomes for days 1st, 3rd, 5th, and 7th of the cell culture have been obtained.

A significance level of $p < 0.001$ is denoted by (***) in the results.

4.3.3. Fluorescence Imaging

(Figure 4.11.) illustrates cell proliferation and attachment on days 3rd and 7th of the cell culture. The cells residing on the scaffolds were stained utilizing AO and PI dyes combined at a 1:1 (v/v) volume ratio. As depicted in (**Figure 4.11.**), the fibroblast cells exhibited their characteristic morphology throughout the cell culture duration. Within the fluorescence micrographs, viable cells are represented in green, while cells with compromised membrane integrity appear red.

From (**Figure 4.11.**), it is discernible that cell density was relatively low for each sample on day 3rd but escalated by day 7th. Moreover, the fluorescence images align with the MTT assay outcomes. For instance, on the 3rd day of cell culture, the quantity

of viable cells on the 1 min. DBD (DAP) PCL/PCL scaffold was the most diminished compared to other samples, while the 5 min. DBD (DAP) PCL/PCL exhibited the highest viable cells on the ultimate day of cell culture.

Furthermore, the cell proliferation and attachment on the 5 min. DBD (DAP) PCL/PCL resemble those observed on the electrospun core-shell PCL/PCL micrograph scaffold. This observation implies that by implementing plasma treatment and incorporating DAP monomer into the scaffolds, the cell density in disparate regions can be modulated.

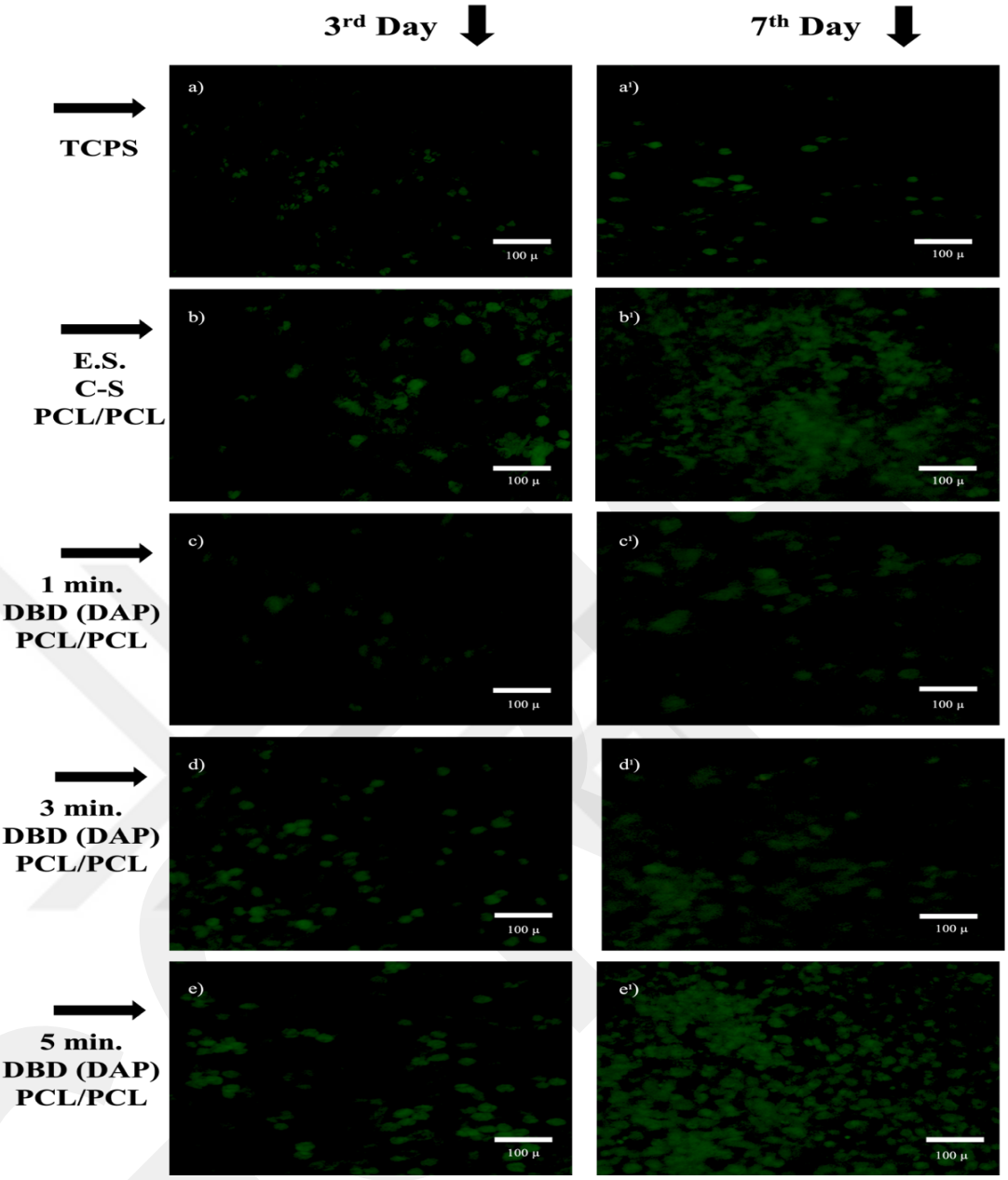

Figure 4.11. Florescence Images of a) TCPS on 3rd day, a¹) TCPS on 7th day, b) E.S. C-S PCL/PCL scaffold on 3rd day, b¹) E.S. C-S PCL/PCL scaffold on 7th day, c) 1 min. DBD (DAP) PCL/PCL scaffold on 3rd day, c¹) 1 min. DBD (DAP) PCL/PCL scaffold on 7th day, d) 3 min. DBD (DAP) PCL/PCL scaffold on 3rd day, d¹) 3 min. DBD (DAP) PCL/PCL scaffold on 7th day. e) 5 min. DBD (DAP) PCL/PCL scaffold on 3rd day, e¹) 5 min. DBD (DAP) PCL/PCL scaffold on 7th day. (All scales are same and shows in 100 µm).

4.3.4. Observation with SEM

The cell attachment and morphology on the fabricated scaffold surfaces were analyzed using SEM. (**Figure 4.12.)** presents the various shapes of L929 fibroblast cells on different samples. For electrospun untreated core-shell PCL/PCL surfaces and those treated with DAP monomer and DBD plasma, SEM images were captured separately from electrospun regions and electrospun areas on plasma-treated surfaces. The SEM images were consistent with fluorescence and MTT assay results, indicating that the DAP monomer incorporated DBD plasma-treated electrospun surfaces had the highest cell count compared to surfaces treated with a shorter DBD treatment time and added DAP at the conclusion of the cell culture period.

The differentiation of cells has been further clarified in the SEM imaging analysis. On day 3rd, L-929 cells exhibited a more spherical, rounder morphology, but by day 7th, cell spreading had occurred. In the SEM images of day 7th, it was understood that the cells adhered to the surface in an anchorage-dependent manner and demonstrated morphological spreading. Additionally, as can be seen from the SEM images, the effects of fiber diameter and surface porosity on the materials are clearly understood.

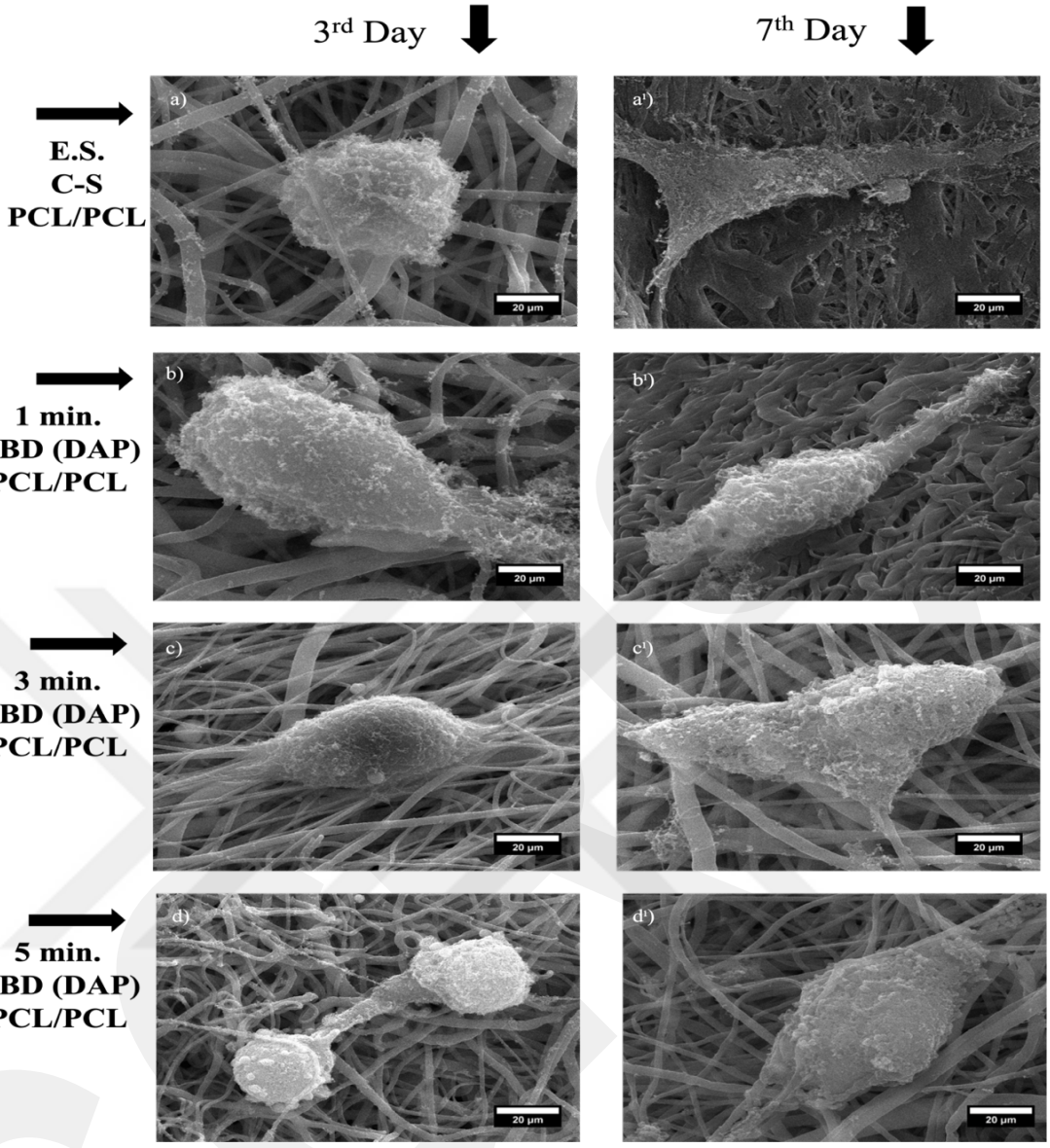

Figure 4.12. SEM images of a) E.S. C-S PCL/PCL scaffold on 3rd day, a') E.S. C-S PCL/PCL scaffold on 7th day, b) 1 min. DBD (DAP) PCL/PCL scaffold on 3rd day, b') 1 min. DBD (DAP) PCL/PCL scaffold on 7th day, c) 3 min. DBD (DAP) PCL/PCL scaffold on 3rd day, c') 3 min. DBD (DAP) PCL/PCL scaffold on 7th day. d) 5 min. DBD (DAP) PCL/PCL scaffold on 3rd day, d') 5 min. DBD (DAP) PCL/PCL scaffold on 7th day. (All scales are same and shows in 20 µm).

CHAPTER 5

Conclusions

- In the conducted study, a core-shell PCL/PCL dental tissue scaffold was produced using the electrospinning method. For sample group 1, the solvent dichloromethane, which exhibits viscous properties, was used in the core, while chloroform, a solvent with lower viscosity, was used to form the shell. Conversely, in sample group 2, the process was reversed; chloroform, a solvent with lower viscosity, was used in the core, and dichloromethane, a solvent with higher viscosity, was used in the shell. The studies were initiated with both experimental groups, and based on the results of the TEM (Transmission Electron Microscopy) image analysis, the experimental work continued with sample group 2, which formed the core-shell structure.

- For sample group 2, the production parameters were prepared as 2 wt% PCL/PCL, with chloroform solvent in the core and DCM solvent in the shell. Successful "Taylor Cone" formation and emission results during the core-shell electrospinning process were achieved when the feeding rate of the shell was 2 (μL/Min) and the feeding rate of the core was 10 (μL/Min), with a voltage value of 20 kV, effectively at a distance of 15 cm from the needle tip.

- The thickness measurement ranges for sample group 1 and sample group 2 show similarity within their respective groups. For sample group 1, the thickness of the non-DBD plasma-treated core-shell PCL/PCL specimen was measured as 0.020 ± 0.002 mm, while the thickness results of the non-DBD plasma-treated core-shell PCL/PCL specimen belonging to sample group 2 was measured as 0.022 ± 0.002 mm. In the Average Fiber Diameter measurements obtained from SEM and TEM images, the lowest value for sample group 2 was 0.452+0.001 (μm) for the non-DBD plasma-treated core-shell PCL/PCL specimen with DAP monomer-treated surfaces, while the highest value for sample group 2 was 0.569 ± 0.002 (μm), which belonged to the core-shell

- PCL/PCL specimen treated with DBD plasma for 5 minutes. In the Average Inter-fiber Pore Size measurements, the non-DBD plasma-treated core-shell PCL/PCL specimen was measured as 2.039 ± 0.503 (μm) as the lowest value, while the core-shell PCL/PCL specimen with a measurement value of 2.160 ± 0.602 (μm), whose surfaces were treated with DAP monomer with DBD plasma for 5 minutes, had the highest pore size.

- The study's findings provide valuable insights into the surface modification of electrospun PCL/PCL nanofibers for dental tissue scaffolds. The surface modifications were carried out using Ar gas + DAP, at argon gas flow rates of 60, 80, and 100 sccm and plasma application times ranging from 0.5 to 5 minutes. The application of plasma surface modifications for over 5 minutes was found to introduce hydrophilicity to the surfaces but also led to excessive etching, making the samples overly hydrophilic and flow damaged, hence unsuitable for dental tissue scaffolds. In contrast, modifications under 1 minute did not significantly alter the hydrophilicity but instead increased the hydrophobicity. Utilizing the DBD Plasma technique proved to be instrumental in demonstrating the influence of DAP coating on the surfaces of the PCL/PCL nanofibers. Ultimately, the optimal hydrophilicity, without any physical or chemical damage, was achieved with 80 and 100 sccm argon flow rates applied for 1 minute. These findings underscore the importance of optimizing the conditions of plasma treatment to balance the hydrophilic and hydrophobic properties of the fibers, crucial for the production of effective dental tissue scaffolds.

- The Contact Angles (CA) of samples treated under specific conditions were slightly above 80°, a decrease of about 10° compared to untreated samples, indicating increased hydrophilicity due to topographical changes and plasma effects. Stable CA values, observed from the sixth day onwards, underscored the ability of the DBD plasma method to significantly enhance surface hydrophilicity. The performance of this method was validated by contrasting untreated scaffolds, which exhibited hydrophobic properties with a CA above 90°, against DAP monomer-coated PCL/PCL surfaces, which showed extreme

hydrophilicity due to DBD plasma. The ultimate aim of the plasma modifications is to match the surface wettability of commercial TCPS, with a CA of 49,7°. DBD plasma treatment parameters were optimized for both untreated and DAP-coated samples, with treatment durations of 1, 3, and 5 minutes. Subsequent wettability analyses were performed over 1 to 8 days, with daily CA measurements, revealing surface-dependent and production time-dependent CA variations. Still, a general trend of increased hydrophilicity compared to untreated samples was noted. The most stable surface property throughout the 8-day study was exhibited by a sample treated with DBD plasma for 5 minutes at 100 sccm. This emphasizes the pivotal role of plasma treatment in manipulating the surface properties of PCL/PCL scaffolds for enhanced applicability in dental tissue engineering.

- Scanning Electron Microscopy (SEM) was utilized to observe the morphology of the nanofibers, revealing the formation of continuous, homogenous structures in the electrospun PCL/PCL nanofibers. Following the DBD plasma method and DAP monomer coating, the core-shell scaffolds exhibited smooth and uniform morphology. Crucially, SEM images disclosed the surface changes, such as increased roughness, and the emergence of cracks, pores, and other surface features post DBD plasma treatment. These alterations, dependent on various factors including treatment time, power, and gas type, as well as initial PCL sample characteristics, underline the profound effect of DBD plasma treatment on PCL/PCL sample surface properties.

- The mechanical properties of untreated and DBD plasma-treated core-shell PCL/PCL nanofibers were significantly different. Untreated nanofibers exhibited an Elastic Modulus of 4.940 ± 0.002 and Tensile Strength of 3.265 ± 0.001. However, after DBD plasma treatment using DAP for 1, 3, and 5 minutes, nanofibers showed changes in these values: Elastic Modulus of 3.825 ± 0.002, 2.952 ± 0.001, 2.171 ± 0.001 and Tensile Strength of 7.652 ± 0.002, 5.020 ± 0.001, 2.156 ± 0.002 respectively. This can be attributed to the smoother surface of the scaffolds due to DBD plasma surface etching, resulting in reduced nanofiber diameters and shorter fracture points.

- The FTIR spectra for both untreated and DBD plasma-treated electrospun core-shell PCL/PCL samples indicated key characteristic bands. The untreated PCL/PCL samples showed bands at specific cm^{-1} values, including symmetric νCH2 stretching, asymmetric νCH2 band, νC-H band, νC=O carbonyl group band, νCH2 bending, νC-O-C ester linkage, νO-C-C stretching band, and νC-C stretching in the crystalline region.

- DBD plasma-treated samples showed similar peak intensities to the untreated samples. However, a time-dependent change was observed in the νP=O peaks due to the phosphate group of the DAP monomer, which accelerated in the 1100-1200 cm^{-1} range. This strengthening of phosphate bonds led to an increase in the peak intensity of the νP=O band over time. Moreover, the stretching intensities of the νP-O-C band were found to increase, demonstrating the influence of DAP monomer on both phosphate and alkyl groups. After the DBD plasma technique was applied, νP=O band was identified between 1250 and 1260 cm^{-1}, and νP-O-C band varied between 900 and 1100 cm^{-1}, suggesting an increase in phosphate and alkyl groups.

- The DBD plasma treatment with DAP resulted in intensified νP=O and νP-O-C peaks and enhanced νC=C peak intensities. The changes induced by DBD plasma and DAP monomer improved the hydrophilicity of the samples, as evident from the CA (°) values. This improvement is instrumental in enhancing biocompatibility, cell attachment on the surface, and drug delivery capabilities, as observed in the study.

- The untreated electrospun PCL/PCL nanofibers absorbed the least amount of PBS, around 70-71%, due to their relatively hydrophobic nature. However, DBD plasma treatment with DAP on the nanofiber surface increased the PBS absorption due to increased hydrophilicity: 5-minute treatment resulted in the highest absorption, about 81-83%; 3-minute treatment followed with approximately 79-80%; and 1-minute treatment had about 75-77% absorption.

- The highest WVTR value belonged to the Electrospun core-shell PCL/PCL scaffolds, which had their surfaces modified with DAP monomer using the DBD plasma method for 5 min. The increase in the average inter-fiber pore size in the electrospun core-shell PCL/PCL scaffolds that were modified with DAP monomer for 5 minutes significantly supported the results obtained here.

- The impact of these developed materials on cell adhesion and growth was investigated using MTT assay methods and fluorescence staining-imaging and SEM imaging. The electrospun core-shell PCL/PCL scaffolds, which had their surfaces modified with DAP monomer for 5 minutes, provided the highest cell growth and proliferation at the end of the culture. In addition, the 3D network of these fabricated core-shell PCL/PCL scaffolds offered cells a higher surface to volume ratio, leading to increased cell density.

REFERENCES

[1] Caton, J. G., & Zander, H. A., "The attachment between tooth and gingival tissues after periodic root planing and soft tissue curettage", *Journal of Periodontology*, vol. 50(9), pp. 462-466, 1979.

[2] Gottlow, J., Nyman, S., Lindhe, J., Karring, T., & Wennström, J., "New attachment formation in the human periodontium by guided tissue regeneration Case reports", *Journal of Clinical Periodontology*, vol. 13(6), pp. 604-616, 1986.

[3] Bottino, M. C., & Thomas, V., "Membranes for periodontal regeneration-a materials perspective", *Biomaterials for Oral and Craniomaxillofacial Applications*, vol. 17, pp. 90-100, 2015.

[4] Rajasekaran, R., Seesala, V. S., Sunka, K. C., Ray, P. G., Saha, B., Banerjee, M., & Dhara, S., "Role of nanofibers on MSCs fate: influence of fiber morphologies, compositions and external stimuli", *Materials Science and Engineering: C*, vol. 107, pp. 110-218, 2020.

[5] Amirian, J., Sultana, T., Joo, G. J., Park, C., & Lee, B. T., "In vitro endothelial differentiation evaluation on polycaprolactone-methoxy polyethylene glycol electrospun membrane and fabrication of multilayered small-diameter hybrid vascular graft", *Journal of Biomaterials Applications*, vol. 34(10), pp. 1395-1408, 2020.

[6] Sadeghianmaryan, A., Karimi, Y., Naghieh, S., Alizadeh Sardroud, H., Gorji, M., & Chen, X., "Electrospinning of scaffolds from the polycaprolactone/polyurethane composite with graphene oxide for skin tissue engineering", *Applied Biochemistry and Biotechnology*, vol. 191(2), pp. 567-578, 2020.

[7] Laudenslager, M. J., & Sigmund, W. M., "Electrospinning. Encyclopedia of Nanotechnology"; *Springer: Dordrecht*, The Netherlands, pp. 769-775, 2012.

[8] Bae, H. S., Haider, A., Selim, K. K., Kang, D. Y., Kim, E. J., & Kang, I. K., "Fabrication of highly porous PMMA electrospun fibers and their

application in the removal of phenol and iodine", *Journal of Polymer Research*, vol. 20(7), pp. 1-7, 2013.

[9] Zhang, C., Yuan, X., Wu, L., Han, Y., & Sheng, J., "Study on morphology of electrospun poly (vinyl alcohol) mats", *European Polymer Journal*, vol. 41(3), pp. 423-432, 2005.

[10] Matabola, K. P., & Moutloali, R. M., "The influence of electrospinning parameters on the morphology and diameter of poly (vinyledene fluoride) nanofibers-effect of sodium chloride", *Journal of Materials Science*, vol. 48(16), pp. 5475-5482, 2013.

[11] Bhardwaj, N., & Kundu, S. C., "Electrospinning: a fascinating fiber fabrication technique", *Biotechnology Advances*, vol. 28(3), pp. 325-347, 2010.

[12] Wang, T., Zhai, Y., Nuzzo, M., Yang, X., Yang, Y., & Zhang, X., "Layer-by-layer nanofiber-enabled engineering of biomimetic periosteum for bone repair and reconstruction", *Biomaterials*, vol. 182, pp. 279-288, 2018.

[13] Sill, T. J., & Von Recum, H. A., "Electrospinning: applications in drug delivery and tissue engineering", *Biomaterials*, vol. 29(13), pp. 1989-2006, 2008.

[14] Sultanova, Z., Kaleli, G., Kabay, G., & Mutlu, M., "Controlled release of a hydrophilic drug from coaxially electrospun polycaprolactone nanofibers", *International Journal of Pharmaceutics*, vol. 505(1-2), pp. 133-138, 2016.

[15] Ha, Sung-Ho & Choung, Pill-Hoon., "MSM promotes human periodontal ligament stem cells differentiation to osteoblast and bone regeneration." *Biochemical and Biophysical Research Communications*, vol. 528, pp. 167-168, 2020.

[16] Kaleli-Can, G., Özgüzar, H. F., Kahriman, S., Türkal, M., Göçmen, J. S., Yurtcu, E., & Mutlu, M., "Improvement in antimicrobial properties of titanium by diethyl phosphite plasma-based surface modification", *Materials Today Communications*, vol. 25, pp.101, 2020.

[17] Jia, E., Zhao, X., Lin, Y., & Su, Z., "Protein adsorption on titanium substrates and its effects on platelet adhesion", *Applied Surface Science*, vol. 9, pp. 225-232, 2020.

[18] Akdoğan, E., & Mutlu, M., "Generation of amphoteric surfaces via glow-discharge technique with single precursor and the behavior of bovine serum albumin at the surface", *Colloids and Surfaces B: Biointerfaces*, vol. 89, pp. 289-294, 2012.

[19] Hilt, F., Duday, D., Gherardi, N., Frache, G., Didierjean, J., & Choquet, P., "Plasma polymerisation of an allyl organophosphate monomer by atmospheric pressure pulsed-PECVD: insights into the growth mechanisms", *RSC Advances*, vol. 5(6), pp. 4277-4285, 2015.

[20] Jacobs, T., Morent, R., De Geyter, N., Dubruel, P., & Leys, C., "Plasma surface modification of biomedical polymers: influence on cell-material interaction", *Plasma Chemistry and Plasma Processing*, vol. 32(5), pp. 1039-1073, 2012.

[21] Borcia, G., Anderson, C. A., & Brown, N. M. D., "Dielectric barrier discharge for surface treatment: application to selected polymers in film and fibre form", *Plasma Sources Science and Technology*, vol. 12(3), pp. 335, 2003.

[22] Azimi, H., Tavakoli, M., & Sharifian, M., "Effect of dielectric barrier discharge (DBD) plasma treatment on the polypropylene film in presence of air and nitrogen at atmospheric pressure", *Advances in Applied NanoBio-Technologies*, vol. 2(2), pp. 41-48, 2021.

[23] Žigon, J., Petrič, M., & Dahle, S., "Dielectric barrier discharge (DBD) plasma pretreatment of lignocellulosic materials in air at atmospheric pressure for their improved wettability: a literature review", *Holzforschung*, vol. 72(11), pp. 979-991, 2018.

[24] Song, J., Chen, Y., & Xia, Y., "Dental tissue engineering and regenerative medicine: A review of current status and future perspectives." *Journal of Dental Research,* vol. 96(4), pp. 388-397, 2017.

[25] Huang, G. T., & Mao, J. J., "Principles of tissue engineering." *Elsevier,* vol. 12, pp. 43-54, 2016.

[26] Wang, Y., Chen, X., & Wang, Y., "Dental tissue engineering: A review of recent progress and future perspectives." *Acta Biomaterialia*, vol. 76, pp. 1-12, 2018.

[27] Park, J. B., & Kim, K. H., "Dental tissue engineering for the regeneration of dental and craniofacial tissues.", *Tissue Engineering and Regenerative Medicine*, vol. 15(2), pp. 93-104, 2018

[28] Da Silva, L. A., & Teixeira, F. B., "Stem cells and scaffolds in dental tissue engineering." *Frontiers in Bioengineering and Biotechnology*, vol. 3, pp. 38, 2015.

[29] Haider, U., & Strickland, D., "Tissue engineering of the oral cavity: A review." *Journal of Dentistry,* vol. 38(12), pp. 905-913, 2010.

[30] Lai, W., & Hutmacher, D. W., "Scaffold-based tissue engineering for craniofacial applications.", *Journal of Dental Research*, 90(3), 259-268.

[31] Lee, Y. K., Kim, Y. J., & Kim, H. J., "Scaffold materials for dental tissue engineering." *Materials Science and Engineering: R: Reports*, vol. 74, pp. 53-87, 2013.

[32] Sun, L., Yang, Y., & Chen, G., "Dental tissue engineering using scaffold-based approaches.", *Journal of dental research*, vol. 94, pp. 905-918, 2015.

[33] Hutmacher, D. W., "Scaffold design and fabrication technologies for engineering tissues.", *Progress in Polymer Science*, vol. 35, pp. 562-599, 2010.

[34] Lu, H., Zhang, Y., & Du, Y., "Dental tissue engineering and regeneration: A review.", *Journal of Tissue Engineering and Regenerative Medicine*, vol. 9(12), pp. 851-862, 2015.

[35] Nam, K.H., et al., "Collagen scaffolds derived from a marine source and their biocompatibility." *Biomaterials*, vol. 24(13), pp. 2565-2571, 2003.

[36] Kajahn, J., et al., “Chitosan-based scaffolds for the regeneration of periodontal tissue.” *Journal of Clinical Periodontology*, vol. 37(10), pp. 883-891, 2003.

[37] Jin, G., et al., “Poly (lactic-co-glycolic acid) microspheres as controlled-release systems for BMP-2.” *Journal of Controlled Release*, vol. 102(1), pp. 35-44, 2005.

[38] Bumgardner, J.D., et al., “Poly(ε-caprolactone) porous scaffolds for tissue engineering.“ *Journal of Biomedical Materials Research*, vol. 61(1), pp. 132-137, 2002.

[39] Costa-Pinto, A.R., et al., “Advances in dental tissue engineering.” *Journal of Biomedical Materials Research Part A*, vol. 92(1), pp. 299-307, 2010.

[40] Gorrasi G. et al., “Correlations between microstructural characterization and thermal properties of well defined poly(ε-caprolactone) samples by ring opening polymerization with neutral and cationic bis (2,4,6-triisopropylphenyl)tin (IV) compounds.”, *Reactive And Functional Polymers*, vol. 70, pp. 151-158, 2010.

[41] Labet M, Thielemans W., “Synthesis of polycaprolactone: a review.” *Chemical Society Revision,* vol. 38:pp. 484-504, 2009.

[42] Wei X. et al., “Biodegradable poly(ε-caprolactone) –poly (ethylene glycol) copolymers as drug delivery system.”, *International Journal of Pharmacy*, vol. 381, pp. 1-8, 2009.

[43] Sinha VR. et al., “Poly-ε-caprolactone microspheres and nanospheres: an overview.”, *International Journal of Pharmacy,* vol. 278, pp. 1-23, 2004.

[44] Wang, J., Li, J., Chen, X., & Zhang, L., “The effects of plasticizers on the properties of hydrogels for tissue engineering.”, *Acta Biomaterialia*, vol. 65, pp. 99-109, 2018.

[45] Zhang, H., Lu, Y., Liu, Y., & Wang, J., “A review of the applications of plasticizers in hydrogels for tissue engineering.”, *Journal of Materials Science & Technology*, vol. 36(7), pp. 1347-1355, 2020.

[46] Chen, J., Li, J., Zhang, L., & Chen, X., “The effects of plasticizers on the properties of hydrogels for tissue engineering.”, *Acta Biomaterialia*, vol. 55, pp. 267-278, 2017.

[47] Li, J., Chen, X., & Zhang, L., “The effects of plasticizers on the properties of hydrogels for tissue engineering.”, *Acta Biomaterialia,* vol. 46, pp. 126-137, 2016.

[48] Taylor G., “Electrically driven jets.”, *Proceeding Royal Society of London*, vol. 313, pp. 453-475, 1969.

[49] Adomaviciute E, Rimvydas M., “The influence of applied voltage on poly (vinyl alcohol) (PVA) nanofibre diameter.”, *Fibers Texting East Europa,* vol. 15, pp. 64–6, 2007..

[50] Huang ZM. et al., “A review on polymer nanofibers by electrospinning and their applications in nanocomposites.”, *Composite Science Technology*, vol. 63, pp. 223-253, 2003.

[51] Thompson CJ. et al., “Effects of parameters on nanofiber diameter determined from electrospinning model.”, *Polymer*, vol. 48, pp. 913-922, 2007.

[52] Shenoy SL. et al., “Role of chain entanglements on fiber formation during electrospinning of polymer solutions: good solvent, non-specific polymer–polymer interaction limit.”, *Polymer* ,2005; vol. 46 ,pp. 372-384, 2005.

[53] Koski A, Yim K, Shivkumar S., “Effect of molecular weight on fibrous PVA produced by electrospinning.”, *Latin Amrerican Journal of Material*, vol. 58, pp. 493-497, 2004.

[54] Baumgarten PK., “Electrostatic spinning of acrylic microfibers.”, *Journal of Colloid Interface Science*, vol. 36, pp. 71-79, 1971.

[55] S. Sukigara, M. Gandhi, J. Ayutsede, M. Micklus and F. Ko., "Regeneration of Bombyx mori silk by electrospinning-part 1: processing parameters and geometric properties", *Polymer,* vol. 44, pp. 5721-5727, 2003.

[56] Tan SH. et al., “Systematic parameter study for ultrafine fiber fabrication via electrospinning process.”, *Polymer,* vol. 46, pp. 128-134, 2005.

[57] Zhang C. et al., “Study on morphology of electrospun poly (vinyl alcohol) mats.”, *Eurasia Polymer Journal*, vol. 41, pp. 423-432, 2005.

[58] Doshi J, Reneker DH., “Electrospinning process and applications of electrospun fibers.”, *Journal of Electrostatics*, vol. 35, pp. 151-160, 1995.

[59] Yuan XY. et al., “Morphology of ultrafine polysulfone fibers prepared by electrospinning.”, *Polymer International*, vol. 53, pp. 704-710, 2004.

[60] Touny AH, Bhaduri SB., “A reactive electrospinning approach for nanoporous PLA/monetite nanocomposite fibers.”, *Material Science Engineering*, vol. 30, pp. 304-312, 2010.

[61] Matthews JA. et al., “Electrospinning of collagen nanofibers.”, *Biomacromolecules*, vol.3, pp. 232-238, 2002.

[62] Carnell LS. et al., “Aligned mats from electrospun single fibers.”, *Macromolecules,* vol.41, pp. 345-349, 2008.

[63] D.M. Shear, J.D. Powell., “The use of wound dressings in dentistry.”, *Journal of the American Dental Association*, vol.13, pp. 1-8, 2019.

[64] P.J. Robinson, J.D. Naylor., “Wound healing in the oral cavity: a review of current concepts.”, *British Journal of Oral and Maxillofacial Surgery*. Vol. 47, pp. 135-147, 2003.

[65] L.M. Edgar., “The use of occlusive dressing in the management of oral wounds.” *Journal of Wound Care*, vol. 30, pp. 143-146, 1999.

[66] Simões D, Miguel SP, Ribeiro MP, Coutinho P, Mendonça AG, Correia IJ., “Recent advances on antimicrobial wound dressing: A review.”, *European Journal of Pharmaceutics and Biopharmaceutics*, vol. 127, pp. 130-141, 2018.

[67] A. Palaia, S. Sfondrini., The effect of wound dressings on pain and healing following oral surgery: a systematic review. Journal of Oral and Maxillofacial Surgery. 2014.

[68] Winter, J., et al. Dielectric barrier discharge plasmas: from fundamentals to applications. Plasma Processes and Polymers, vol. 12, no. 1, 2015, pp. 1–26.

[69] M Moisan, J Barbeau, S Moreau, J Pelletier, M Tabrizian, L'H Yahia,, "Low-temperature sterilization using gas plasmas: a review of the experiments and an analysis of the inactivation mechanisms,", *International Journal of Pharmaceutics*,, vol. 226, pp. 1-21, 2001.

[70] Wei, M., et al., "Plasma Surface Modification of Polycaprolactone Films for Enhanced Cell Adhesion and Proliferation.", *Journal of Biomedical Materials Research Part A*, vol. 105, pp. 943–952, 2016.

[71] Wang, Y., et al., "Surface modification of polycaprolactone films by dielectric barrier discharge plasma for improved wettability and cell attachment.", *Journal of Applied Polymer Science*, vol. 134,pp. 45-74, 2017.

[72] Sun, Y., et al., "Effect of dielectric barrier discharge plasma treatment on the surface characteristics and biocompatibility of polycaprolactone films.", *Journal of Biomedical Materials Research Part A*, vol. 102, pp. 538–547, 2014.

[73] R. Jain, S. Shetty, and K.S. Yadav, "Unfolding the electrospinning potential of biopolymers for preparation of nanofibers", *Journal of Drug Delivery Science and Technology* , vol. 57, pp. 463-484 2020.

[74] H. Sasmazel and O. Ozkan, "Advances in Electrospinning of Nanofibers and their Biomedical Applications", *Current Tissue Engineering*, vol. 2, pp. 91–108, 2013.

[75] Huang, Y., & Shi, S., "Dental tissue engineering: A review of current status and future prospects.", *Regenerative Medicine*, vol. 5, pp. 343-357, 2010.

[76] Bielefeld, K. A., Amini-Nik, S., and Alman, B. A., "Cutaneous wound healing: recruiting developmental pathways for regeneration.", *Cellular and Molecular Life Sciences,* vol. 70, pp. 2059–2081, 2013.

[77] Cooper, D. M., “Wound healing: new understandings.”, *Nurse Practice Forum* vol. 10, pp. 74–86, 1999.

[78] Diegelmann, R. F., and Evans, M. C., “Wound healing: an overview of acute, fibrotic and delayed healing.”, *Front Range Biosciences,* vol. 9, pp. 283–289, 2004.

[79] Gharaee-Kermani, M., and Phan, S. H., “Role of cytokines and cytokine therapy in wound healing and fibrotic diseases.”, *Current Pharmaceutical Design,* vol. 7, pp. 1083–1103, 2001.

[80] Mutschler, W., “Physiology and pathophysiology of wound healing of wound defects.”, *Unfallchirurg,* vol. 115, pp. 767–773, 2012.

[81] Velnar, T., Bailey, T., and Smrkolj, V., “The wound healing process: an overview of the cellular and molecular mechanisms.”, *Journal of International Medical Researches,* vol. 37, pp. 1528–1542, 2009.

[82] Vanwijck, R., “Surgical biology of wound healing.”, *Académie Royale de Medecine de Belgique*, vol. 156, pp. 175–184, 2001.

[83] Discepoli, N., Vignoletti, F., Laino, L., de Sanctis, M., Muñoz, F., and Sanz, M., “Early healing of the alveolar process after tooth extraction: an experimental study in the beagle dog.” *Journal of Clinical Periodontology,* vol. 40, pp. 638–644, 2013.

[84] Moraschini, V., and Barboza, E. S., “Effect of autologous platelet concentrates for alveolar socket preservation: a systematic review.”, *International Journal of Oral Maxillofacial. Surgery,* vol. 44, pp. 632–641, 2015.

[85] Goldberg, M., “Pulp healing and regeneration: more questions than answers.” *Advances in Dental Researches,* vol. 23, pp. 270–274, 2011.

[86] Kirsner, R. S., and Eaglstein, W. H., “The wound healing process.” *Dermatological Clinics,* vol. 11, pp. 629–640, 1993.

[87] Sørensen, L. T., “Wound healing and infection in surgery: the pathophysiological impact of smoking, smoking cessation, and nicotine replacement therapy: a systematic review.”, *Annals Surgery,* vol. 255, pp. 1069–1079, 2012.

[88] S. Surucu and H. Turkoglu Sasmazel, “Development of core-shell coaxially electrospun composite PCL/chitosan scaffolds” *International Journal of Biological Macromolecules*, vol. 92, pp. 321–328 (2016).

[89] Annual Book of ASTM Standards, “ASTM E96: Standard Test Methods for Water Vapor Transmission of Materials.”, 1995, pp. 785-792.

[90] Eda D. Yildirim, H. Ayan, V. N. Vasilets, A. Fridman, S. Guceri, W. Sun, “Effect of Dielectric Barrier Discharge Plasma on the Attachment and Proliferation of Osteoblasts Cultured over Poly(ε-caprolactone) Scaffolds.” *Plasma Processes and Polymers*., vol. 5, pp. 58-66, 2007.

[91] Gümüşderelioğlu M, Türkoğlu H., “Biomodification of non-woven polyester fabrics by insulin and RGD for use in serum-free cultivation of tissue cells.” *Biomaterials*, vol. 23, pp. 3927–3935, 2002.

[92] Sun Z. et al., “Compound core–shell polymer nanofibers by co-electrospinning.” *Advanced Materials*, vol. 22, pp. 1929-1932, 2003.

[93] Ma, Z., Kotaki, M., Inai, R., & Ramakrishna, S., “Potential of nanofiber matrix as tissue-engineering scaffolds.”, *Tissue Engineering*, vol. 11, pp. 101-109, 2005.

[94] T. C. Lee, H. C. Chen, C. Y. Lee, and Y. H. Tseng, "Surface modification of electrospun polycaprolactone fibers using dielectric barrier discharge plasma treatment," *Materials Letters*, vol. 62, pp. 980-983, 2008.

[95] S. Tang, W. Zhao, X. Lu, H. Li, and X. Tang, "Surface modification of electrospun polycaprolactone (PCL) nanofibers with dielectric barrier discharge plasma for enhancement of cell proliferation," *Applied Surface Science*, vol. 311, pp. 429-434, 2014.

[96] Kim, J. H., Shin, J. W., Kim, B. H., Lee, J. W., & Kim, Y. H. "FTIR analysis of electrospun PCL nanofibers with DBD plasma treatment.", *Journal of Nanoscience and Nanotechnology*, vol. 15, pp. 1537-1540, 2015.

[97] Li, Y., Li, L., Li, X., Li, X., & Li, J. "Characterization of DAP-based flame retardant thermoplastic polyurethane: FTIR, XRD and TGA.", *Journal of Analytical and Applied Pyrolysis*, vol. 122, pp. 61-67, 2016.

[98] Tauer, K., Le, T. N., & Garsuch, A. "Functionalized polyacrylamide as electrolyte for electrochemical energy storage.", *Macromolecular Chemistry and Physics*, vol. 216, pp. 1405-1413, 2015.

[99] Kuo, C.-H., Lu, T.-Y., Chang, S.-J., & Liu, Y.-L. "Effects of argon plasma treatment on the surface properties of poly(ε-caprolactone) electrospun membranes.", *Journal of Biomaterials Applications*, vol. 30, pp. 379-392, 2015.

[100] Wu, Y., Li, L., Li, Q., Li, J., Li, D., Li, Y., & Wang, X. "Effects of argon plasma treatment on surface morphology, structure, and properties of poly(ε-caprolactone) electrospun fibers.", *Journal of Biomedical Materials Research Part A*, vol. 106, pp. 2563-2573, 2018.

[101] Han, D.; Steckl, A. "Coaxial Electrospinning Formation of Complex Polymer Fibers and Their Applications." *ChemPlusChem*, vol. 84, pp.1453-1497, 2019.

[102] Aragon, Javier, Navascues, Nuria, Mendoza, Gracia, Irusta, Silvia, "Laser-treated electrospun fiber loaded with nano-hydroxyapatite for bone tissue engineering", *International Journal of Pharmaceutics*, vol. 4, 112-122, 2017.

[103] Seda Surucu & Hilal Turkoglu Sasmazel, "DBD atmospheric plasma-modified, electrospun, layer-by-layer polymeric scaffolds for L929 fibroblast cell cultivation.", *Journal of Biomaterials Science, Polymer Edition*, vol. 27, pp. 111-132, 2016.

[104] S. Surucu, K. Masur, H. Turkoglu Sasmazel, T. Von Woedtke, and K.D. Weltmann, "Atmospheric plasma surface modifications of electrospun PCL/chitosan/PCL hybrid scaffolds by nozzle type plasma jets for usage of cell cultivation" *Applied Surface Science*, vol. 385, pp. 400–409, 2016.

[105] Albayrak, D., Turkoglu Sasmazel, H., "Surface patterning of poly(ε-caprolactone) scaffolds by electrospinning for monitoring cell biomass behavior.", *Journal of Polymer Researchers*, vol. 29, pp. 339, 2022.

[106] Teuta Eljezi, Pierre Pinta, Damien Richard, Jérémy Pinguet, Jean-Michel Chezal, Marie-Christine Chagnon, Valérie Sautou, Gaël Grimandi, Emmanuel Moreau, "In vitro cytotoxic effects of DEHP-alternative plasticizers and their primary metabolites on a L929 cell line.", *Chemosphere*, vol. 173, pp. 452-459, 2017.

[107] Mosmann T, "Rapid Colorimetric Assay for Cellular Growth and Survival: Application to Proliferation and Cytotoxicity Assays.", *Journal of Immunologic Methods*, vol. 65, pp. 55–63, 1983.

[108] Kısmalı, G., Sel, T, "Paraquat ile Oluşturulmuş Oksidatif Stresin HepG2 Hücrelerinde Apoptozis Üzerine Etkisinin Araştırılması.", *Fırat Üniversitesi Sağlık Bilimleri Veteriner Dergisi*, vol. 26, pp. 79- 85, 2012.